Extraction and accuracy assessment of high-resolution DEM and derived orthoimages from ALOS-PRISM data over Sahel-Doukkala (Morocco)

Habib, Adnane; Akdim, Nadia; El Ghandour, Fatima ezzahra; Labbassi, Kamal; Khoshelham, Kourosh; Menenti, Massimo

DOI
10.1007/s12145-017-0287-5

Publication date
2017

Document Version
Final published version

Published in
Earth Science Informatics

Earth Sci Inform (2017) 10:197–217
DOI 10.1007/s12145-017-0287-5

RESEARCH ARTICLE

Extraction and accuracy assessment of high-resolution DEM and derived orthoimages from ALOS-PRISM data over Sahel-Doukkala (Morocco)

Adnane Habib[1] · **Nadia Akdim**[1] · **Fatima-ezzahra El Ghandour**[1] · **Kamal Labbassi**[1] · **Kourosh Khoshelham**[2] · **Massimo Menenti**[3]

Received: 5 July 2016 / Accepted: 9 January 2017 / Published online: 14 January 2017

Abstract In Sahel-Doukkala, which is characterized by lands of a relatively low relief, global DEMs and DEMs generated from digitizing topographic maps, have been the primary source of several multidisciplinary researches. Although these products present a great value of the conducted research, the level of the given accuracy is not sufficient enough for detailed geospatial analysis. These requirements led us to generate a high-resolution DEM as an alternative of available global DEMs or/and DEMs generated from digitizing topographic maps. In this study, we present a workflow to extract high-resolution DEM at 5 m resolution and derived orthoimages from ALOS-PRISM data over Sahel-Doukkala, through photogrammetric techniques, using a variation of GCPs obtained from topographic maps at scale 1:25,000. The accuracy of the generated products is reported according to NSSDA standards. Using ten GCPs, a PRISM-DEM with 3.88 m vertical accuracy and 11.60 m horizontal accuracy, both at 95% confidence level is obtained. This DEM will serve as base dataset for further detailed geospatial analysis and mapping applications in order to identify the relationship between surface parameters and groundwater, and also to assess and understand all factors influencing the development of karst landscapes and consequently subsurface stability in the investigated area.

Keywords ALOS-RISM · DEM · Orthoimage · Accuracy assessment · Sahel-Doukkala, Morocco

Responsible editor: H. A. Babaie

✉ Adnane Habib
adnanehabib@gmail.com

[1] LGMSS-URAC45, Department of Earth Sciences, Faculty of Science, Chouaïb Doukkali University, Route Ben Maâchou, 24000 El Jadida, Morocco

[2] Department of Infrastructure Engineering, University of Melbourne, Melbourne 3010, Australia

[3] Geosciences and Remote Sensing Department, Delft University of Technology, Stevinweg 12628 CN, Delft, The Netherlands

Introduction

Problem statement

Over the last decade, Sahel-Doukkala (Western Morocco) was under an increasing pressure from intense and rapid change in land use/land cover (LULC) due to a growing demographic, touristic, agricultural, and industrial activities. This change in LULC has a direct impact on land resources; particularly groundwater, where the water demand has significantly amplified, while water resources are increasingly scarce. Therefore, this is considered as a major problem affecting this region, where groundwater is the only water supply resources. Furthermore, the interference of this LULC change with the local geomorphological, structural, geological and hydrological factors, shapes the landscape, i.e. karst landscapes, leading to the formation of cavities and underground drainage system, thus threatening the subsurface stability of this area. Therefore, it shows the necessity to conduct investigation efforts to better understand the relationship between groundwater and subsurface information, and also to understand all factors influencing the development of karst landscapes and consequently subsurface stability. These studies will provide valuable tools for better planning, monitoring and management of land resources, especially groundwater, and karst landscapes in Sahel-Doukkala.

This kind of studies requires the calculation of several geomorphometric parameters such as elevation, slope, drainage density, terrain features, etc. Nowadays, such information can be easily obtained trough Digital Elevation Model (DEM) which becomes the main source of information on topography (Florinsky 2012). The quality of such analysis is controlled by the quality of the DEM. For this reason, a DEM with high and consistent accuracy (horizontal and vertical) is preferable. Currently, different global DEMs with different resolution and accuracy are freely-available such as SRTM (Shuttle Radar Topography Mission) and ASTER GDEM (Advanced Spaceborne Thermal Emission and Reflection Radiometer (ASTER) Global Digital Elevation Model (GDEM)). Through the release of SRTMGL1 (Farr et al. 2007; NASA JPL 2013), with a spatial resolution of 30 m and a vertical accuracy about 16 m, it is considered more sensitive to elevation variation compared to others free global DEMs, and it becomes the first choice. However, this level of accuracy is not sufficient enough for detailed geospatial analysis, especially in areas with relatively low relief, where a DEM with higher accuracy is more preferred. Ground surveying techniques using GNSS systems and airborne LiDAR surveys are the most accurate techniques for DEM generation (Persendt and Gomez 2015; Migoń and Kasprzak 2015), nevertheless, difficulties such as time-consuming and high expenses are still the major constraint. In such circumstances DEMs from satellite imagery are a worthwhile option.

A digital elevation model (DEM) is a 3D digital representation of a terrain surface, created from elevation data. There are two types of DEMs, digital terrain model (DTM) and digital surface model (DSM). A DTM represents the elevation associated with the topography of the Earth, excluding all man-made and keeps only natural features while DSM represents the elevation associated with the Earth's surface, including all objects on it (man-made and natural features). In scientific literature, the term of DEM is used as a generic term for DTM and DSM (Li et al. 2005). DEMs generated from aerial photographs, satellite imagery (ASTER, SPOT, ALOS-PRISM, Cartosat-1, ERS SAR, Envisat ASAR, TerraSAR-X, etc), LiDAR or provided by global suppliers (such as USGS) are in fact DSMs. DSM can be converted to DTM by applying several algorithms that try to remove all elevated features (Kraus and Pfeifer 1998; Vosselman 2000; Sithole and Vosselman 2004; Krauß et al. 2011; Bandara et al. 2011). However, in the following decades, the use of the concepts DEM, DTM and/or DSM has been confusing, and the use of this terms have a context-dependent implication and there may be differences in meaning from one country to another (Oksanen 2006). In the following, the term DEM is referred to DSM.

In Sahel-Doukkala, which is characterized by lands of a relatively low relief, global DEMs such as SRTM and ASTER DEM, and DEMs generated by interpolation between contours and spot heights from existing topographic maps, have been the primary source of several multidisciplinary research (Labbassi et al. 2009; El Bchari et al. 2014; Theilen-Willige et al. 2014; Fadili et al. 2015). Although these products present a great value for the conducted studies, the level of the given accuracy is not sufficient enough for detailed geospatial analysis, especially in the case of a relatively low relief. Moreover, it is crucial to assess the overall accuracy requirements of DEM before any geospatial analysis. However, these requirements are not defined in spite of the common use of DEMs, and there is still a lack of research involving an accuracy assessment studies and methods of those DEMs over Sahel-Doukkala. This contribution will contribute to better understanding of the error components and the overall accuracy of a high-resolution DEM in this area.

These requirements led us to conduct this research in order to generate a high-resolution DEM as an alternative of available global DEMs or/and DEMs generated from digitizing topographic maps. In addition, an accuracy assessment of the generated DEM is performed in order to better understand the error components of the DEM, the propagated error in each component, the bias of error, and the overall accuracy. The obtained DEM will serve as a basic elevation product for further geospatial analysis and orthorectification of additional remote sensing datasets.

Motivation

With the advent of very high-resolution (VHR) optical satellites with stereoscopic sensors, e.g. ALOS-PRISM, SPOT-7, GeoEye-1/2, WorldView-1/2, Cartosat-1/2, etc., spatial images can have a resolution inferior than 5 m. With this very high resolution, spatial images gained a popularity in the geospatial scientific community and become a principal data source of digital Photogrammetry; which is more integrated into remote sensing and GIScience at the present time, leading to a new era in DEM generation. Therefore, many studies have been conducted using and evaluating VHR optical images as a new alternative for DEM generation (Al-Rousan et al. 1997; Toutin 2004; Büyüksalih et al. 2005; Maruya and Ohyama 2008; Krauß et al. 2009; Bhardwaj 2013; Jacobsen 2013).

The PRISM instrument onboard the Japanese satellite ALOS, with its 2.5 m resolution triplet images, has been designed mainly for mapping purpose with a specific intention towards high-resolution DEM generation. With its unique configuration, ALOS-PRISM gives a strong advantage compared to the conventional stereo imaging system in term of producing accurate DEMs and orthoimages (Maruya and Ohyama 2008). Early results from previous studies available in the scientific literature confirm the high accuracy of generated DEM and derived orthoimages from ALOS-PRISM images. Maruya and Ohyama (2008) used GCPs derived from a 1:25,000 map in order to assess the accuracy of PRISM-DEM and PRISM ortho-rectified images, and found an RMSE of

4.8 m and 5.8 m for PRISM-DEM and Nadir-orthoimage respectively. In another experiment, a standard deviation of 4.07 m for the overall DEM, 5.24 m for the mountainous area and 2.34 m for the plain area was obtained by Bignone and Umakawa (2008) for a comparison with the obtained PRISM-DEM to a DEM generated from IKONOS images. A comparison of height difference between PRISM-DEM and SRTM has been conducted by Trisakti et al. (2009) gives RMSE of 6.5 m. (Takaku et al. 2008) generated PRISM DEMs from several scenes over different sites over Japan, presenting various terrain features (flat, mountainous, steep, urban) and compared the PRISM-DEM accuracy with high-resolution reference DEM derived from LiDAR and aerial photo and found RMSE ranging between 5 m and 21 m.

In this study, photogrammetric methods, more specifically spaceborne Photogrammetry is selected for the availability of data sources and its acceptable accuracy. An advantage of processing of photogrammetric DEM is that it is a standard approach and it has been in use for several decades and is still improving (Nelson et al. 2009). The fundamental principle of Photogrammetry is to make use of a stereopair (two images of the same scene imaged at two slightly different places with a certain degree of overlap) to reconstruct the original shape of 3D objects and then to measure the 3D coordinates of the objects on the derived stereo model (Li et al. 2005).

The main purpose of the present paper is to extract a high-resolution DEM from ALOS-PRISM data trough photogrammetric techniques, and subsequently, generate orthoimages. The approach used is divided into three main steps. The first step is the extraction of PRISM DEMs (called PDEMs). The second step represents an accuracy assessment of the generated PDEMs through different accuracy assessment techniques. Finally, PRISM orthoimages are generated using the final PDEM. The accuracy of PRISM DEMs and PRISM orthoimages are reported according to the NSSDA (National Standard for Spatial Data Accuracy) vertical and horizontal accuracy published by the Federal Geographic Data Committee (FGDC) in 1998, which uses RMSE to estimate positional accuracy at the 95% confidence level (Federal Geographic Data Committee 1998).

Study area

The study area is located in Moroccan Atlantic coast between latitude 33°20'N and 33°15'N and covers an area approximately 45 km by 65 km (Fig. 1). The topography of the area includes two most significant units, the Sahel and the Doukkala. The Sahel, which represents a gently rolling hills with the presence of some local steep slopes, it is a combination and the intercalation of many consolidated dunes. It is characterized by low to moderate relief and regular morphology where the ridges of the dunes follow; over long distances, the same orientation, which is NE-SW and separated by so-called inter-dunes depressions. The elevation of this unit ranges from 0 to 160 m. In addition, the Sahel includes a sub-unit called the Oulja, which is located near to the ocean. This area is a quite big depression containing wetlands and some agricultural fields. The second main geomorphological unit is the Doukkala, which remains as wide plain characterized by very low topographic variation.

Data and tools

PRISM sensor

The Advanced Land Observing Satellite (ALOS), also called DAICHI, is an Earth observation satellite launched on January 24, 2006 by the Japan Aerospace Exploration Agency (JAXA), with onboard PRISM, AVNIR-2 and PALSAR instruments (JAXA 2008). The Panchromatic Remote Sensing Instrument for Stereo Mapping (PRISM) consists of three independent panchromatic radiometers for nadir (NDR), forward (FWD), and backward (BWD) looking. These radiometers produce high-resolution triplet and stereo images along the satellite's track with 2.5 m. Main characteristics of PRISM instrument are shown in Table 1.

The stereo images are captured at nearly the same time; 45 s for two sequential overlap captures, under uniform environmental and lighting conditions. PRISM data are processed in three levels: Level 1A, Level 1B, and Level 1B2, with two observation modes, which are OB1 (triplet mode) and OB2 (dual mode) (Tadono et al. 2004). Forward and backward radiometers are inclined at +/− 23.8 degrees from the nadir to provide a base-to-height (B/H) ratio of 1.0 with triplet mode, and a B/H ratio of 0.5 with dual mode. This ratio is very important for DEM generation process as a larger B/H ratio contributes to a better vertical accuracy (Hasegawa et al. 2000; Kääb 2008).

PRISM dataset description

The scenes used in this study are ordered from ESA (European Space Agency). In this study, two frames were selected over Sahel-Doukkala (orbit 12,988, track 343, frame 2935, and frame 2940) with level 1B1, which is radiometrically corrected and is without geometric correction. This level is considered the most suitable level for DEM generation (Wang et al. 2008). There was acquired on July 2nd, 2008 at about 11:21 a.m. The scenes are available with dual-mode (Forward and Nadir looking) in CEOS format. They cover an area of 35 km × 35 km for each frame, with a spatial resolution of 2.5 m. In the images, lagoon, forest, temporary small lakes, agricultural field, hills, and flat terrains are visible. These frames present a good quality with free cloud and they are delivered with full metadata ((Fig. 2)

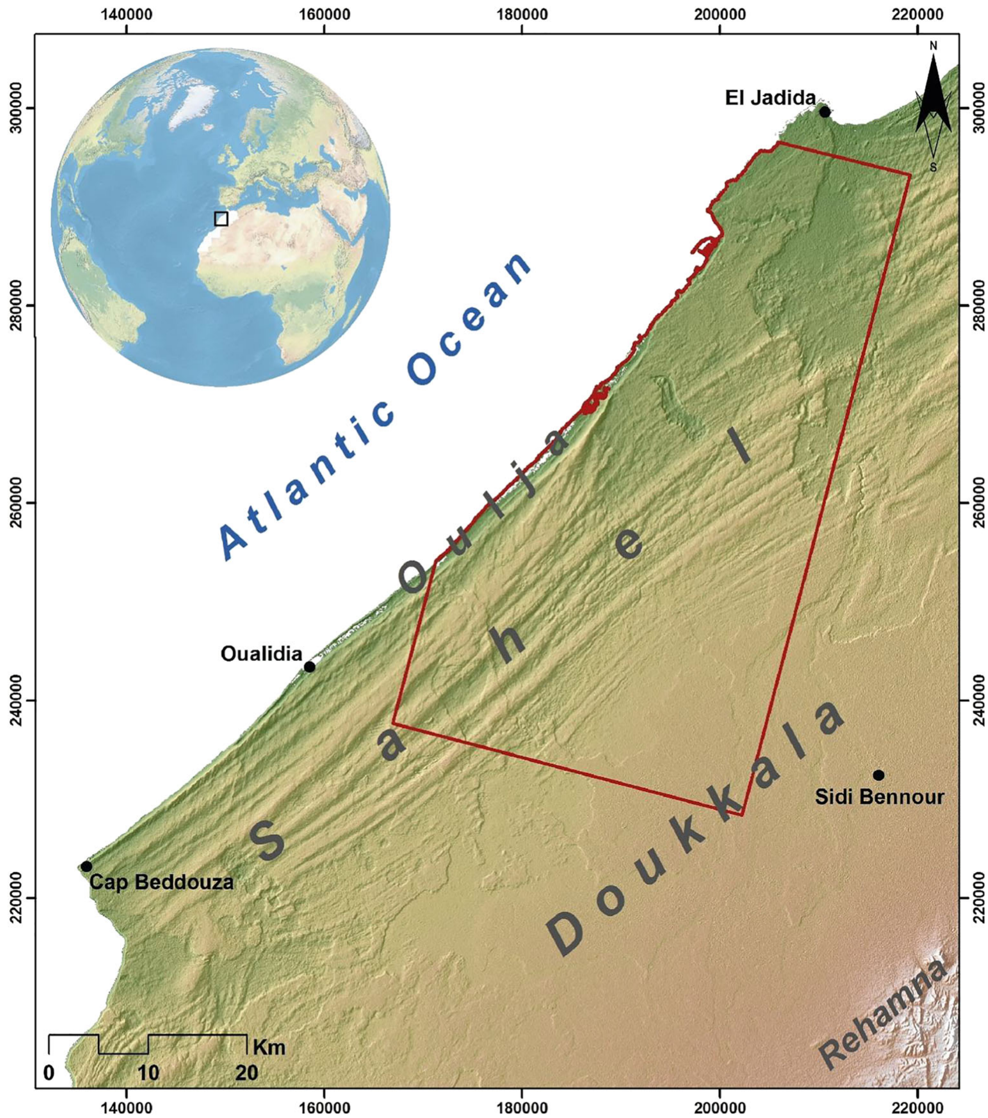

Fig. 1 The location of the study area (red box)

Ground control points

In order to orient the final DEM to a recognized map projection and to compute the Exterior Orientation Parameters (EOPs), a sufficient number of GCPs is required. In addition, GCPs are needed as an independent source of information to check the accuracy and the consistency of photogrammetric derived product.

In our case, it was not possible to acquire Geodetic GPS survey measurements. As an alternative, it was decided to use published topographic maps by the Moroccan Cartographic Survey (ANCFCC) as the main resource for the collection of GCPs and validation points (vertical and horizontal). The used topographic maps are at scale 1:25,000; which remain the best source of GCPs over the study area with a planimetric accuracy of 5 m and altimetric accuracy of 2.5 m, were georeferenced in ArcGIS using Lambert Conformal Conic of Morocco (LCCM) as projection system (Fig. 3).

SRTMGL1

The Shuttle Radar Topography Mission (SRTM) was a collaboration between the National Aeronautics and Space Administration (NASA) and the National Geospatial-Intelligence Agency (NGA) (previously known as the National Imagery and Mapping Agency (NIMA)), with a participation of the German Aerospace Center (DLR), and the Italian Space Agency (ASI). The mission was designed to use a single-pass radar interferometer to produce a DEM of the Earth's land surface (about 80% of the globe) between about 60° North latitude and 56° South latitude which launched February 11th , 2000 and flew for 11 days aboard

Table 1 Specifications of PRISM instrument (JAXA 2008)

Item	Description
Number of observation bands	1 (Panchromatic)
Wavelength	0.52 to 0.77 μm
Number of optics	3 (Forward (FWD) – Nadir (NDR) – Backward (BWD))
B/H	1.0 (triplet mode) – 0.5 (dual mode)
Spatial resolution	2.5 m (at NDR)
FOV (Swath Width)	70 km (NDR only) / 35 km (Triplet mode)
S/N	>70
MTF	>0.2
Angle from NDR	±23.8° (for FWD and BWD Along track direction)
Bit length	8 bits
Observation frequency	0.37 ms
IFOV	3.61 μrad
Pointing angle	±1.5° (Triplet mode, cross-track direction)

the space shuttle endeavor (Farr et al. 2007). C-Radar data were processed at JPL (Jet Propulsion Laboratory), while X-Radar data (DLR & ASI) were processed at DLR.

The NASA data products are distributed free of charge to the public through the USGS EROS Data Center. In the United States, data were made available at 1 × 1 arc-Sec (approximately 30 m at the equator), which was produced by averaging 3 × 3 pixels. For the rest of the world, a lower resolution (3 arc-sec - approximately 90 m at the equator) for global data set called SRTM3 was produced. The vertical error of the SRTM is reported to be less than 16 m for 90% of the data across the entire mission and less than 5 m on a local scale (Rabus et al. 2003; Gonçalves 2005; Jacobsen 2005; Rodriguez et al. 2005; Farr et al. 2007; Mukherjee et al. 2013). Since September 2014, the White House has announced that the high-resolution topographic data generated from NASA's SRTM in 2000 will be released globally and publicly over 2014 and the beginning of 2015 (NASA 2014). This enhanced SRTM version, called SRTMGL1 (NASA Shuttle Radar Topography Mission Global 1 arc sec) was released with 1 arc-second (about 30 m) revealing the full resolution of the original measurements taken by NASA's SRTM mission.

The SRTM DEM can be a good alternative source for elevation comparison and assessment for regions where DGPS survey measurements or accurate topographic maps are not available (Rozycki and Wolniewicz 2007). It was also used as source of height information in several parts of the world where collection of height information was impossible (Galiatsatos et al. 2008; Gonçalves 2008).

Software used

In this paper, it was decided to use IMAGINE Photogrammetry module (formerly Leica Photogrammetry Suite) implemented in ERDAS IMAGINE Software. IMAGINE Photogrammetry has the ability to handle ALOS-PRISM data format with level 1B1 and provides full chain for automatic DEM generation. ArcGIS and SAGA GIS were used for GIS operation such as georeferencing, GIS spatial analysis, and terrain parameters extraction

Methodology and workflow

The approach used in this work was divided into three main steps. After the image orientation, an image matching, and automatic DEM generation were performed. Then an accuracy assessment of the generated PDEMs was achieved through different accuracy assessment techniques. Finally, PRISM orthoimages were generated using the final obtained PDEM. The methodology is summarized by the flowchart diagram shown in Fig. 4.

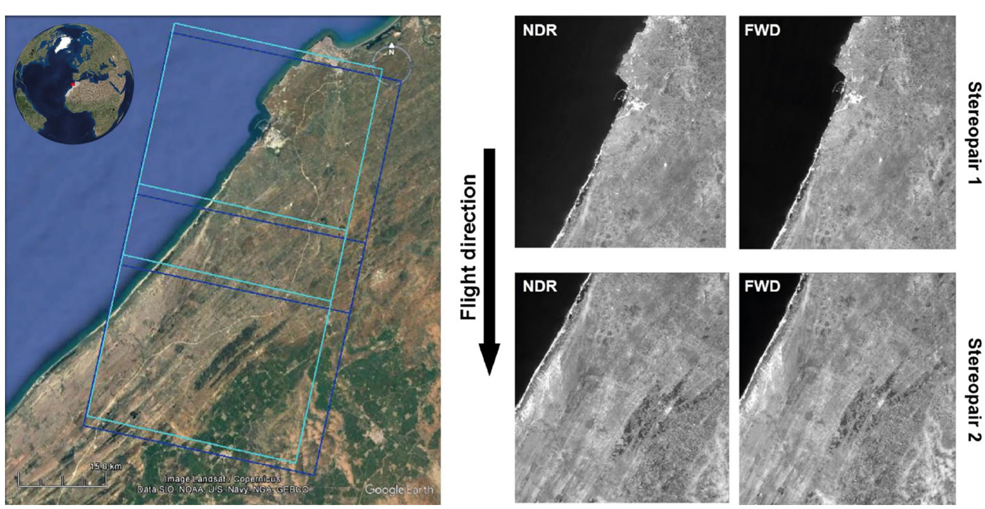

Fig. 2 Footprint and overview of used ALOS-PRISM data (cyan frames present nadir scenes, while blue frames present forward scenes) (Credit: Google Earth)

Fig. 3 Spatial distribution of ALOS-PRISM images, topographic maps, ground control points (GCPs), vertical checkpoints (VCPs) and orthoimages validation points over the study area

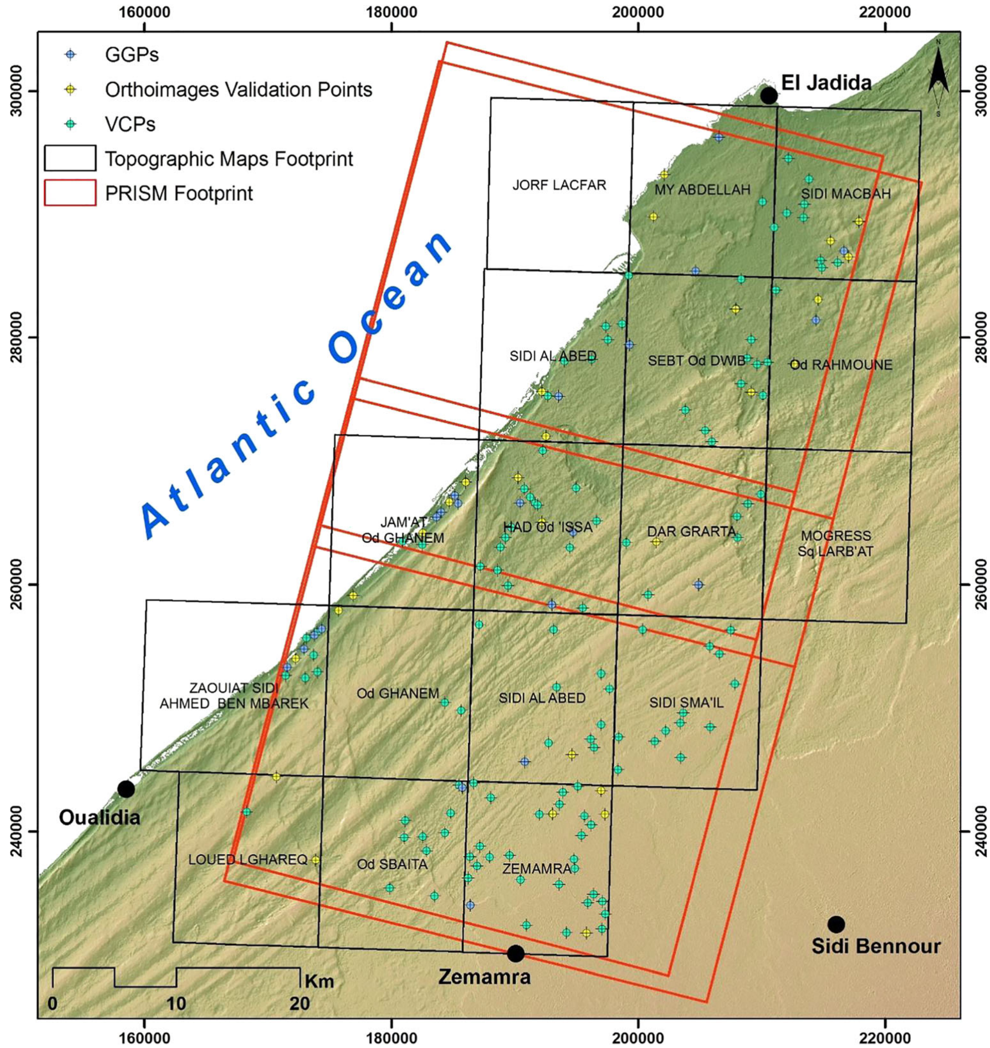

DEM generation

Preprocessing

The initial settings were the selection of an appropriate sensor model and the reference system. Considering the GCPs source (topographic maps), it was decided to use the same reference system, which is LCCM (Lambert Conformal Conic of Morocco). Furthermore, in order to achieve reasonable results in term of accuracy and reliability in DEM generation, a coarse-to-fine hierarchical strategy based on image pyramids was built.

Image orientation

Sensor model determination In the image orientation processing, the determination of the sensor model is a crucial step. ALOS-PRISM L1B1 data are delivered with full metadata including detailed sensor parameters, satellite ephemeris information (orbital position and velocity), and satellite attitude information (rotation angles). That's why, the orbital pushbroom sensor model is considered as the most suitable model for ALOS-PRISM L1B1 data, which fully utilizes this information to determine IOPs and EOPs to satisfy the modified collinearity equation. This information is read directly by IMAGINE Photogrammetry and used in the creation of the block files.

However, EOPs from ephemeris and attitude information cannot be accurate enough to build the model, which depend on the accuracy of ephemeris and attitude information. To overcome this problem, an additional adjustment of the model can be performed using known GCPs. Theoretically, a minimum of 3 full GCPs determined and located on each stereopair are sufficient to solve the 6 parameters for EOPs and to orient the images. Nevertheless, to increase the accuracy of the block, more GCPs have to be collected (Wegmann 2002; Galiatsatos et al. 2008; Michalis and Dowman 2008; Bitelli and Girelli 2009; Kocaman and Gruen 2009). These points are used with the BBA (Bundle Block Adjustment), where all images are oriented simultaneously in the same reference system.

Fig. 4 Flowchart of the followed approach

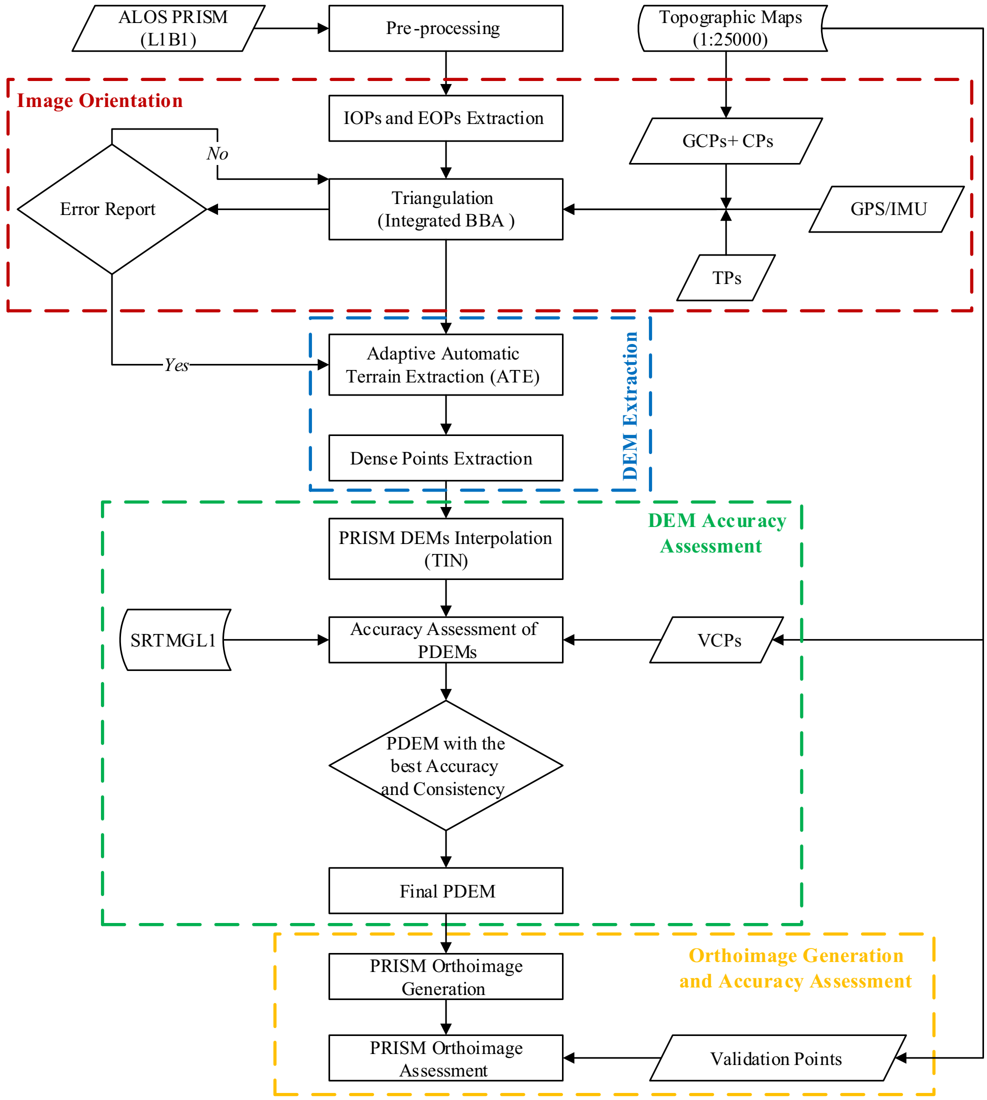

GCPs collection In DEM generation process, GCPs should satisfy two conditions: (i) the accuracy of GCPs should be high enough. (ii) GCPs should be identifiable and locatable in each image of the block. In our case, full GCPs (X, Y, Z) are collected from 1:25,000 topographic maps, which remain our best alternative. In order to straightforwardness their identification, they are usually determined close to the road crossing and intersection of agricultural plots. Because of the difference in information content between ALOS-PRISM images and topographic maps, it was very difficult to define good common recognizable points between them. To overcome this limitation, a total of 112 reference points was collected having a good distribution on the images, and located at different elevations, to avoid planimetric and altimetric extrapolations (Toutin 2001) (Fig. 3), with the intention to reduce this number and keep only the best reference points.

Triangulation The orbital Pushbroom sensor model associated with PRISM images was designed to give results with no significant error; without any adjustment, by means of only ephemeris and attitude information. Nevertheless, to improve the sensor model and get better results, the adjustment of the block is quite required, by using known full GCPs and tie points.

Triangulation was performed using integrated BBA, which uses the collinearity equation as formula and have the advantage of distributing the error over the entire block. Reference points collected from topographic maps separated into two categories: GCPs were used to perform triangulation and Check Points (CPs) which were not used to contribute in resolving the sensor model but used to independently verify the overall accuracy of BAA. There are considered as the best source for determining the accuracy of the BBA. Also, the triangulation process needs the collection of several correspondences points, called Ties Points (TPs), between the stereo images via an image matching algorithm.

In order to improve the sensor model, we tried to use several variations of GCPs, in order to find the optimal one which will improve the overall accuracy of the block by reducing gross errors from image point measurement. In the first triangulation trial, all reference points were used. Then, based on the triangulation report, GCPs with large residuals were removed in order to reduce and avoid gross errors from image point measurement. In the final stage, the best GCPs were kept in order to be used in triangulation.

A total of 21 reference points were retained of which 15 points were used as GCPs and 6 points were used as CPs. The number of reference points retained was the best possible under the given conditions. Afterward, different experiments of triangulation were performed using zero, 3, 6, 10, and 15 GCPs.

In a previous study conducted by Khoshelham (2009), it has been shown that including tie points within an integrated orientation approach, i.e. BBA, can result in a reduction of errors in the image space. Hence, an automatic TPs generation was performed, where a total of 202 points was generated.

Image matching and DEM extraction

Once the orientation was completed, ALOS-PRISM images can be used for automatic DEM generation through image matching algorithm. With known sensor orientation parameters, automatic image matching techniques are able to extract dense point cloud describing the ground surface and its main geometric discontinuities.

IMAGINE Photogrammetry software uses a hierarchical feature based multi-image matching technique and an adaptive automatic terrain extraction (ATE) for DEM generation. After matching on each pyramid level, the terrain is refined, gross errors are removed and a more accurate and detailed terrain serves as the input of next pyramid level correlation (Wang et al. 2008). The search window size used to search corresponding image points was set to 11 × 3, while the correlation size was set to 11 × 11, and the correlation coefficient was adjusted to 0.9 (Lane et al. 2000; Leica Geosystems Geospatial Imaging 2006; Milledge et al. 2009). At the same time, a DEM filter was used to remove the erroneously matched points from the output 3D points.

Four different DEMs were extracted and called PDEM3T, PDEM6T, PDEM10T, PDEM15T for, respectively 3 GCPs, 6 GCPs, 10 GCPs, and 15 GCPs. The generated DEMs were stored as point cloud presenting the raw DEM values computed from the matched image points. Afterward, Delaunay Triangulation was performed to create TIN (Triangulated Irregular Network) from the output 3D points, and then it was spatially interpolated using a linear surface fitting algorithm to obtain DEM with 5 m pixel size. TIN is an exact interpolation where original data points are kept without any bias. Also, it is efficient for representing sudden changes in topography, and areas with uniform slope and aspect (McCullagh 1988; Jordan 2007).

Accuracy assessment

In order to evaluate the generated PDEMs, many accuracy assessment techniques were used, which are: error difference statistics, spatial correlation and regression analysis, image differencing, profiling analysis, and topographic analysis (Hirano et al. 2003; Eckert et al. 2005; San and Suzen 2005; Galiatsatos et al. 2008; Lamsal et al. 2011; Pulighe and Fava 2013).

The accuracy of PDEMs was reported according to NSSDA vertical accuracy, which uses RMSEz (in z-component) to estimate positional accuracy at the 95% confidence level (Federal Geographic Data Committee 1998). This accuracy is a linear uncertainty value, such that the true or theoretical location of the point falls within ± of that linear uncertainty value 95% of the time, in other words, it means that 95% of all the computed points have an error with respect to the true measurement that is smaller or equal to the stated accuracy.

The NSSDA vertical accuracy assumes that systematic errors have been eliminated as best as possible. Furthermore, if vertical errors are normally distributed, the factor 1.9600 is applied to compute linear error at the 95% confidence level. Consequently, vertical accuracy, $accuracy_z$, reported according to the NSSDA shall be computed by the following formula (Federal Geographic Data Committee 1998):

$$Accuracy_z = 1.9600 * RMSE_z \quad (1)$$

Where:

$Accuracy_z$ *is the vertical accuracy at the 95% confidence interval*

And

$$RMSE_z = \sqrt{\frac{\sum_{I-1}^{n} \left(z_{\text{data } I} - z_{\text{check } I}\right)^2}{n}} \quad (2)$$

Where:

$z_{data\ I}$ *is the vertical coordinate of the I^{th} checkpoint in the dataset*

$z_{check\ I}$ *is the vertical coordinate of the I^{th} checkpoint in the independent source of higher accuracy*

n *is the number of checkpoints tested*

I *is an integer ranging from 1 to n*

The generated PDEMs were firstly evaluated using 143 well distributed vertical checkpoints (VCPs) extracted from 1:25,000 topographic maps (Fig. 3). Elevations at the locations of VCPs was extracted from generated PDEMs and compared with the elevations of VCPs in order to perform several statistical analyses. First, descriptive statistics of generated

PDEMs and VCPs were performed. Then PDEMs were compared to VCPs by calculating the difference between them, where a statistical analysis of the errors was performed.

Rather than checking the accuracy on local points, which gives only the only amount of the errors, the global PDEMs were compared to a reference DEM, through image differencing approach. This technique leads to the detection and quantification of error's distribution over the entire PDEM. In this study, it was decided to choose SRTMGL1 as reference DEM.

In addition, a profiling evaluation was performed to assess the planimetric accuracy and the variation of errors according to the geomorphology of the study area. Two elevation profiles oriented in NW-SE and NNE-SSW respectively, for each PDEM (PRISM-DEM) and SRTMGL1 were chosen and evaluated.

Slope and aspect; among other topographic features, are two of the most important features that can influence and affect morphological and hydrological pattern of DEMs. They represent the recommended variables to analyze their impact on error distribution. For this purpose, slope and aspect maps for PDEMs were generated, then slope and aspect values at VCPs were extracted from each PDEM. Later, a statistical analysis of PDEMs errors was performed for slope classes and aspect directions.

Orthoimage generation

PRISM orthoimages were made using the nadir images for both stereopairs and PDEM presenting the best accuracy and consistency. Next, in order to assess the geometric registration of PRISM orthoimages, 33 validation points and their corresponding points were selected from road intersection from both topographic maps and orthoimages (Fig. 3). Later, the differences between X and Y values from the validation point; with their known locations, and those defined by the PRISM orthoimages were calculated in order to get the shift (error) for a given validation point with orthoimages. Based on those differences, the $RMSE_{xy}$ and NSSDA horizontal accuracy were calculated to assess the accuracy of the generated orthoimages.

Like PDEMs, the accuracy of PRISM orthoimages was reported according to NSSDA horizontal accuracy which uses $RMSE_{xy}$ (RMSE in x- and y- component) to estimate horizontal positional accuracy at the 95% confidence level. The reporting standard in the horizontal component is the radius of circle of uncertainty, such that the true or theoretical location of the point falls within that circle 95% of the time (Federal Geographic Data Committee 1998) .

The $RMSE_{xy}$ can be divided into two accuracies components, in x- component positional $RMSE_x$ and y- component positional $RMSE_y$, with the following formulas:

$$\mathrm{RMSE}_x = \sqrt{\frac{\sum_{I-1}^{n} \left(x_{\text{data } I} - x_{\text{check } I}\right)^2}{n}} \tag{3}$$

$$\mathrm{RMSE}_y = \sqrt{\frac{\sum_{I-1}^{n} \left(y_{\text{data } I} - y_{\text{check } I}\right)^2}{n}} \tag{4}$$

$x_{data}I$ and $x_{data\ I}$ *are the horizontal coordinates of the* I^{th}*checkpoint in the dataset*

Table 2 Summary of residuals and errors for GCPs and CPs

No. CPs			6				
No. TPs			202				
No. GCPs			15	10	6	3	0
GCPs RMSE	Ground X	Meters	2.838	2.368	3.156	1.092	---
	Ground Y		3.082	2.951	7.695	2.903	---
	Ground Z		2.852	2.110	1.365	1.423	---
	Image X	Pixels	1.170	1.023	1.022	0.627	---
	Image Y		1.221	1.181	2.341	0.8310	---
CPs RMSE	Ground X	Meters	3.804	3.989	4.323	4.035	128.620
	Ground Y		3.699	2.695	9.607	7.370	107.629
	Ground Z		3.070	3.653	5.931	4.429	199.401
	Image X	Pixels	1.379	1.396	0.810	1.108	34.685
	Image Y		1.390	1.207	3.645	2.745	39.621
Total RMSE		Pixels	0.047	0.035	0.041	0.031	---

Table 3 Descriptive statistics of VCPs and generated DEMs

	Min (m)	Max (m)	Mean (m)	Median (m)	SD (m)
VCPs (143)	2.00	176.00	98.31	99.00	45.37
PDEM3T	-5.89	175.25	97.33	98.80	45.94
PDEM6T	-5.72	174.81	97.68	99.42	45.80
PDEM10T	-4.78	173.34	97.40	99.94	45.61
PDEM15T	-4.29	172.17	98.09	100.32	44.17

$y_{check\ I}$ and $y_{check\ I}$ *is the horizontal coordinates of the* I^{th} *checkpoint in the independent source of higher accuracy*

n *is the number of checkpoints tested*

I *is an integer ranging from 1 to n*

The horizontal error at point I is defined as:

$$\text{Error } I = \sqrt{\left(x_{\text{data } I} - x_{\text{check } I}\right)^2 + \left(y_{\text{data } I} - y_{\text{check } I}\right)^2} \tag{5}$$

Then, horizontal RMSE_{xy} is given as below:

$$RMSE_{xy} = \sqrt{\frac{\sum_{I-1}^{n}\left(x_{\text{data } I} - x_{\text{check } I}\right)^2 + \left(y_{\text{data } I} - y_{\text{check } I}\right)^2}{n}} = \sqrt{\left(RMSE_x^2 + RMSE_y^2\right)} \tag{6}$$

The NSSDA standards assume that systematic errors have been eliminated as best as possible. In addition, if horizontal errors are normally distributed and independently in each of the x- and y- component, the factor 2.4477 is applied to compute horizontal accuracy at the 95% confidence level. When the preceding conditions apply, the horizontal accuracy, $accuracy_{xy}$, shall be computed as follows (Federal Geographic Data Committee 1998):

$$Accuracy_{xy} = \frac{2.4477 * RMSE_{xy}}{2} \tag{7}$$

Therefore, this standard implements two formulas to report the total horizontal accuracy, $accuracy_{xy}$, at 95 confidence level.

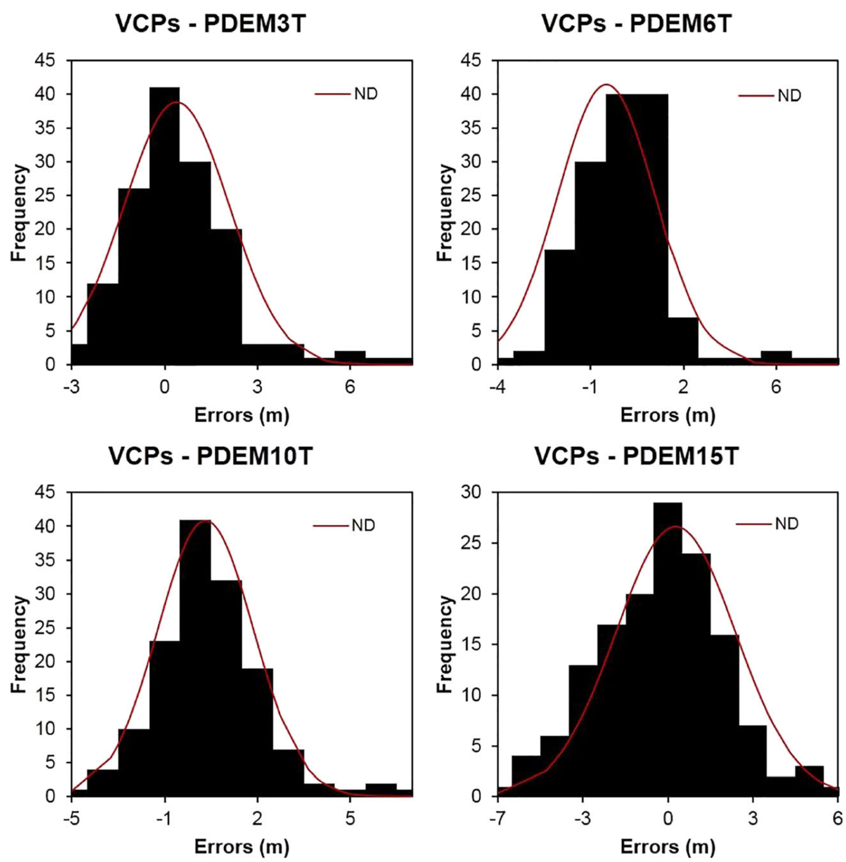

Fig. 5 Histograms of error distribution frequencies of differences between VCPs and generated PDEMs (ND represents the normal distribution)

– **Case1:**

If $RMSE_x = RMSE_y$, the horizontal accuracy can be computed by the following formula:

$$RMSE_{xy} = \sqrt{2*RMSE_x^2} = \sqrt{2*RMSE_y^2} = 1.4142*RMSE_x = 1.4142*RMSE_y \quad (8)$$

$$Accuracy_{xy} = \frac{2.4477*RMSE_{xy}}{1.4142} = 1.7308*RMSE_{xy} \quad (9)$$

– **Case2** (results similar to Case1):

If $RMSE_x \# RMSE_y$, (the ratio between the largest RMSE and the smallest one is between 0.6 and 1.0), then the accuracy can be computed by the following formula:

$$Accuracy_{xy} = \frac{2.4477*(RMSE_x + RMSE_y)}{2} = 1.22385*(RMSE_x + RMSE_y) \quad (10)$$

Where:

$Accuracy_{xy}$ *is the horizontal (radial) accuracy at the 95% confidence interval*

Results and discussion

Different experiments of triangulation were performed using 3, 6, 10, and 15 GCPs collected from topographic maps. Furthermore, an automatic TPs generation was performed, where a total of 202 points was generated. The results were compared with 6 well-defined accurate CPs.

Once the triangulation was performed and EOPs were solved, ground coordinates and image coordinates of GCPs, CPs, and TPs are computed with their corresponding accuracy and are displayed in the triangulation report in the form of residuals (Table 2). The CPs errors are computed from the subtraction of the computed coordinates from the original input coordinates. Since the CPs are not used to build the sensor model, therefore, the model is considered well built, more the errors of the CPs are less significant.

Observing Table 2, when only ephemeris and attitude data were used (0 GCPs), it is seen that the errors of CPs ground coordinates are very large especially for Z. However, when few GCPs were added the six parameters of exterior orientation were corrected and the accuracy of the model can be significantly improved. The overall accuracy of triangulation with 3, 6, 10, and 15 GCPs performs similarly. CPs image coordinates errors are in general within 1 to 3 pixels. Nevertheless, we have to be careful when looking at the errors of CPs. They are not as good as the GCPs since the best points are firstly implemented to improve the sensor model. The residuals of GCPs are much better than CPs, which for image coordinates is mostly within 1 to 2 pixels.

It can be observed that the insertion of just three GCPs can reduce the amount of CPs errors by more than 90% for both image coordinates and ground coordinates. More GCPs can lead to better improvements. In the case of using 10 GCPs, a remarkable enhancement can be observed. Adding more GCPs can improve the model, but with no significant enhancement because the model starts to be saturated. It should be noted that the uncertainty of GCPs and CPs is quite high, but it was the best height control points available at the time.

Table 5 Correlation and regression coefficients between VCPs and generated PDEMs

	r	R^2	Regression line $y = ax + b$	
			Slope (a)	Intercept (b)
PDEM3T	0.99925	0.99851	1.0117	-2.1306
PDEM6T	0.99932	0.99864	1.0086	-1.4766
PDEM10T	0.99926	0.99853	1.0046	-1.3626
PDEM15T	0.99910	0.99820	0.9726	-2.4764

r: Correlation Coefficient

Table 4 Statistical parameters between VCPs and PDEMs

	Min (m)	Max (m)	Mean (m)	Median (m)	SD (m)	MAE (m)	$RMSE_Z$ (m)	ACC_Z 95 (m)
VCPs - SRTMGL1	-8.00	5.00	0.08	0.00	2.36	1.83	2.29	4.48
VCPs - PDEM3T	-2.73	9.28	0.98	0.85	1.85	1.52	2.09	4.09
VCPs - PDEM6T	-3.25	8.90	0.63	0.67	1.74	1.28	1.84	3.61
VCPs - PDEM10T	-4.02	8.53	0.91	0.75	1.76	1.46	1.98	3.88
VCPs - PDEM15T	-6.45	6.29	0.22	0.42	2.25	1.81	2.25	4.41

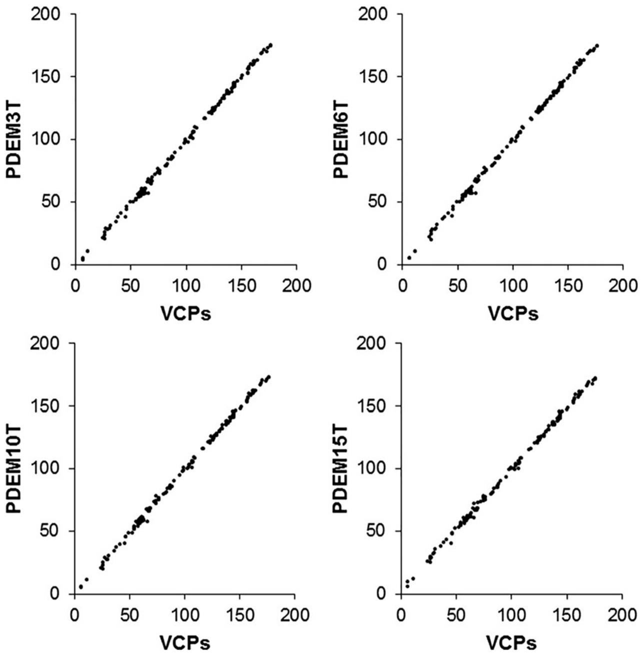

Fig. 6 Correlation plots between elevation values (meters) of VCPs and generated PDEMs

As seen above, it is hard to tell which model is better. For that reason, it was decided to generate DEMs using the different variations of GCPs described above. Four different absolute DEMs were extracted and called PDEM3T, PDEM6T, PDEM10T, and PDEM15T, for 3 GCPs, 6 GCPs, 10 GCPs, and 15 GCPs respectively.

The generated DEMs were first evaluated using 143 well defined vertical checkpoints (VCPs) extracted from 1:25,000 topographic maps (Fig. 3). First the descriptive statistics of both, VCPs and generated PDEMs were calculated (Table 3). From the statistics given in this table, it is perceived that all generated PDEMs are slightly close to VCPs in population measures (mean, median, and standard deviation (SD)), making difficult to state which PDEM is closest to VCPs.

Then, a comparison of the generated PDEMs with VCPs was performed by calculating the difference between VCPs and their corresponding points in the produced PDEMs, which denoted as VCPs – PDEMx. A statistical analysis of errors was achieved by calculating the MAE (Mean Absolute Error), RMSEz and NSSDA vertical accuracy at 95 confidence interval among other parameters such as Min, Max, Mean, Median, and SD. Figure 5 shows the histograms of errors distribution frequencies of difference between VCPs and generated PDEMs, while Table 4 summarizes the statistical parameters between VCPs and PDEMs.

Examination of these results shows that all generated PDEMs present a good agreement with VCPs and the overall range of the errors distribution is quite small, and fit in a remarkable way the normal distribution, where the frequency of positive errors is slightly greater than negative errors, which indicates a small positive bias. Looking at the statistics, even if

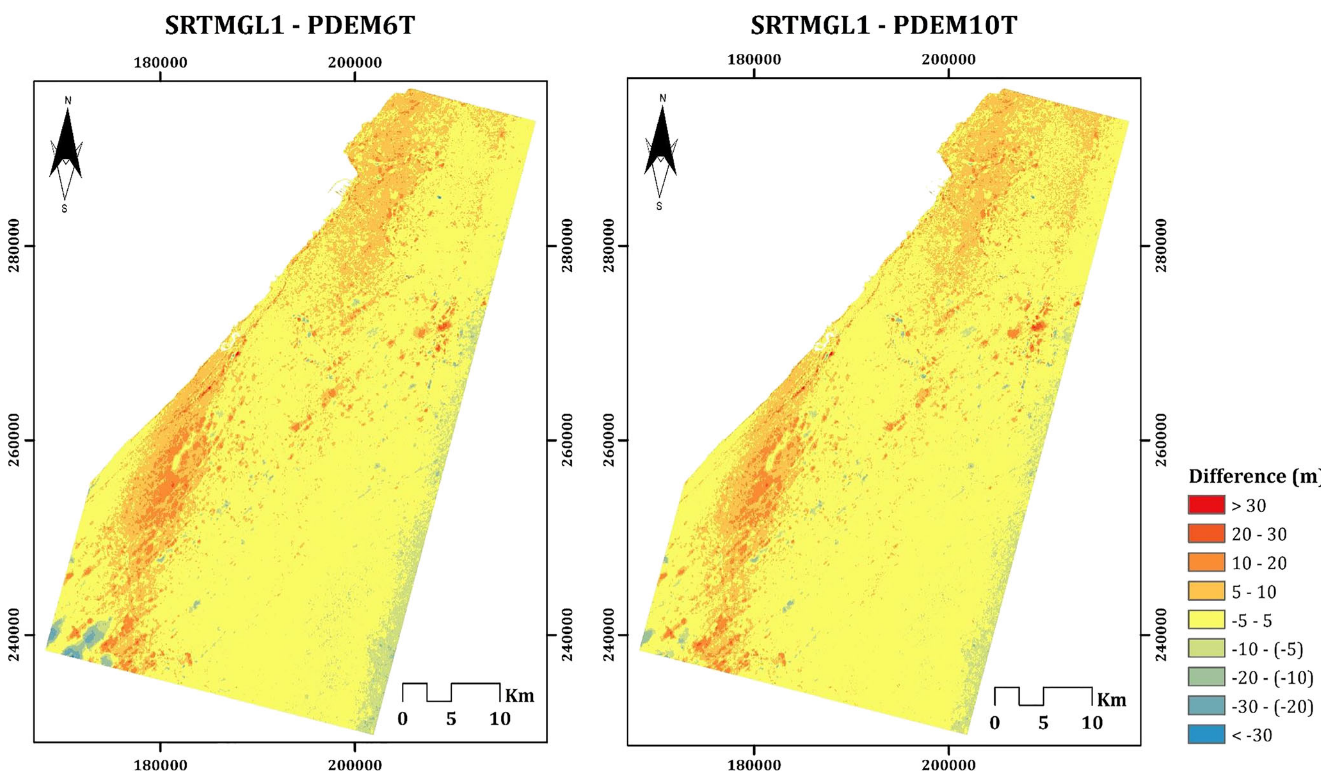

Fig. 7 Elevation difference maps between SRTMGL1 and PDEM6T/PDEM10T

Table 6 Statistical summary of errors between SRTMGL1 and PDEM6T/PDEM10T

	Min (m)	Max (m)	Mean (m)	Median (m)	SD (m)	CI (95%) (m)
SRTMGL1 - PDEM6T	-6.19	7.86	0.64	0.56	2.67	0.45
SRTMGL1 - PDEM10T	-5.50	7.25	0.92	0.62	2.45	0.42

that all generated PDEMs shows a relatively small and acceptable statistic accuracy estimator, PDEM6T and PDEM10T gain immediately our attention since they have the lowest values and a very consistent behavior for the MAE, RMSEz and NSSDA vertical accuracy.

In order to have a better understanding of the relationship between VCPs and PDEMs, spatial correlation and linear regression analysis were calculated (Table 5 and Fig. 6). It is seen that all generated PDEMs have a strong positive correlation exceeding 99% with a very high determination coefficient (R^2), which reveals that the VCPs and the generated PDEMs using TPs are highly correlated to each other.

Consequently, based on the comparison of error difference statistics between VCPs and generated PDEMs, it is found that PDEM6T and PDEM10T had, relatively, the highest vertical accuracy. Also, PDEM6T and PDEM10T present, relatively, the highest correlation with VCPs and they have the smallest linear offset (it is considered that the linear offset is stored in the intercept of the regression equation). Therefore, PDEM6T and PDEM10T are kept for further evaluation with SRTMGL1.

Even if the correlation analysis presents a good correlation between VCPs and both PDEM6T and PDEM10T, this method is limited because it cannot give precise information about the spatial distribution of elevation errors. To overcome this problem, it was decided to use the image differencing approach which leads to have a clear idea of the spatial distribution of errors between a reference DEM (SRTMGL1 in our case) and generated DEM (PDEM6T and PDEM10T), by generating a difference image (error image) through a subtraction technique, where both the amounts and locations of errors are stored as error images.

Direct subtraction of generated PDEMs from SRTMGL1 is problematic because of the difference in spatial resolution between them. To overcome this problem, SRTMGL1 was resampled to the generated PDEMs resolution, and then a difference image (Fig. 7) showing the spatial distribution of the errors was made by subtracting PDEM6T and PDEM10T from SRTMGL1. A statistical analysis of difference maps was made using all overlaid pixels (Table 6). To quantify the dominance of errors, histograms of both difference maps were made (Fig. 8). Then, error pixels were classified using classes with a range of 5 and 10 m, where the number of contained error pixels was calculated and then converted to an error percentage (Table 7).

The difference errors between SRTMGL1 and PDEM6T/PDEM10T follows a normal distribution, with a smaller errors range in the case of the PDEM10T, especially on the negative side. Investigation of difference images statistics shows that both generated PDEMs have a very good error distribution, with a relatively small mean in the case of PDEM6T around 0.64 m, which indicates that the elevation values of PDEM6T are quite higher with around a half of meter than SRTMGL1. While the SD of PDEM10T is smaller than PDEM6T; which indicates how the model is computed differs from the reference, shows that the overall difference between SRTMGL1 and PDEM10T is smaller than the difference between SRTMGL1 and PDEM6T.

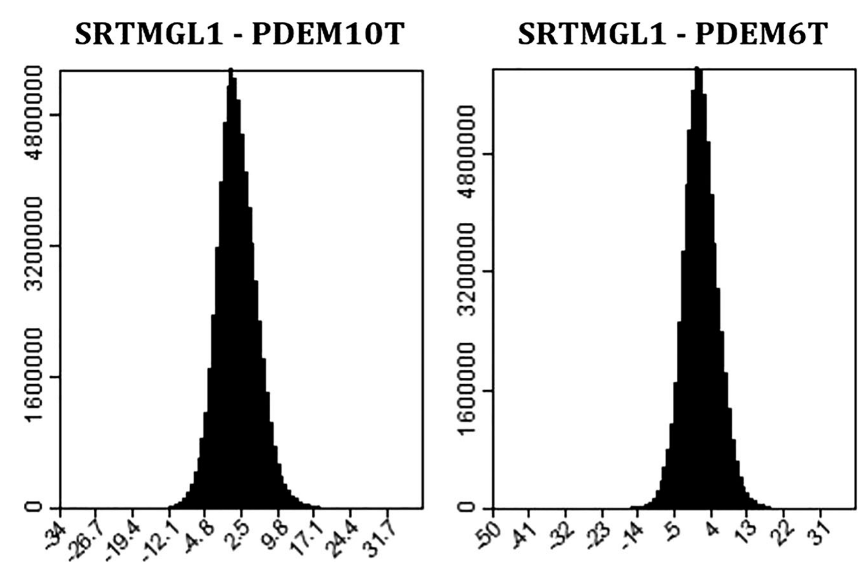

Fig. 8 Histograms of errors between SRTMGL1 and PDEM6T/PDEM10T (x-axis: errors in meters) (y-axis: number of pixels)

Table 7 Elevation errors difference expressed in term of percentage per class

Δh (m)	-30 < Δh < −20	-20 < Δh < −10	-10 < Δh < −5	-5 < Δh < 5	5 < Δh < 10	10 < Δh < 20	20 < Δh < 30
SRTMGL1 - PDEM6T	0.14%	0.66%	4.77%	72.80%	18.05%	3.49%	0.08%
SRTMGL1 - PDEM10T	0.01%	0.29%	3.47%	75.66%	17.65%	2.84%	0.08%

Observing both difference maps, it is observed that most of the areas are colored in medium yellow since the difference errors are largely ranged between −10 and 10 m. The most dominance (majority dominance) class is (−5) – 5 m, which represents 72.80% and 75.66% for PDEM6T and PDEM10T respectively, while the class (−10) – 10 m represents an overwhelming dominance with 95.62% and 96.78% for PDEM6T and PDEM10T respectively. The extreme outliers are obvious where there are red and blue with extreme errors. These are located at the boundaries of the generated PDEMs, over steep slopes (cliff, depressions), areas with poor matching (the left lower part of PDEMs). Also, these differential images show a pattern in flight direction (Y direction of ALOS-PRISM images), which can be probably caused by the sensor model, i.e. IOPs. These errors don't exceed +20 m and represent just 3.49% and 2.83% for PDEM6T and PDEM10T respectively.

Comparing PDEM6T and PDEM10T, it is seen that the amount of elevation errors decreases in the case of PDEM10T, where the major improvement was observed in the lower left corner due to image matching correlation issue, which turns from blue (−30 m) to medium yellow (±10 m). It is also seen that the percentage of error distribution is better in the case of PDEM10T, where 75.66% of the errors is in ±5 m range and 96.78% in ±10 m range.

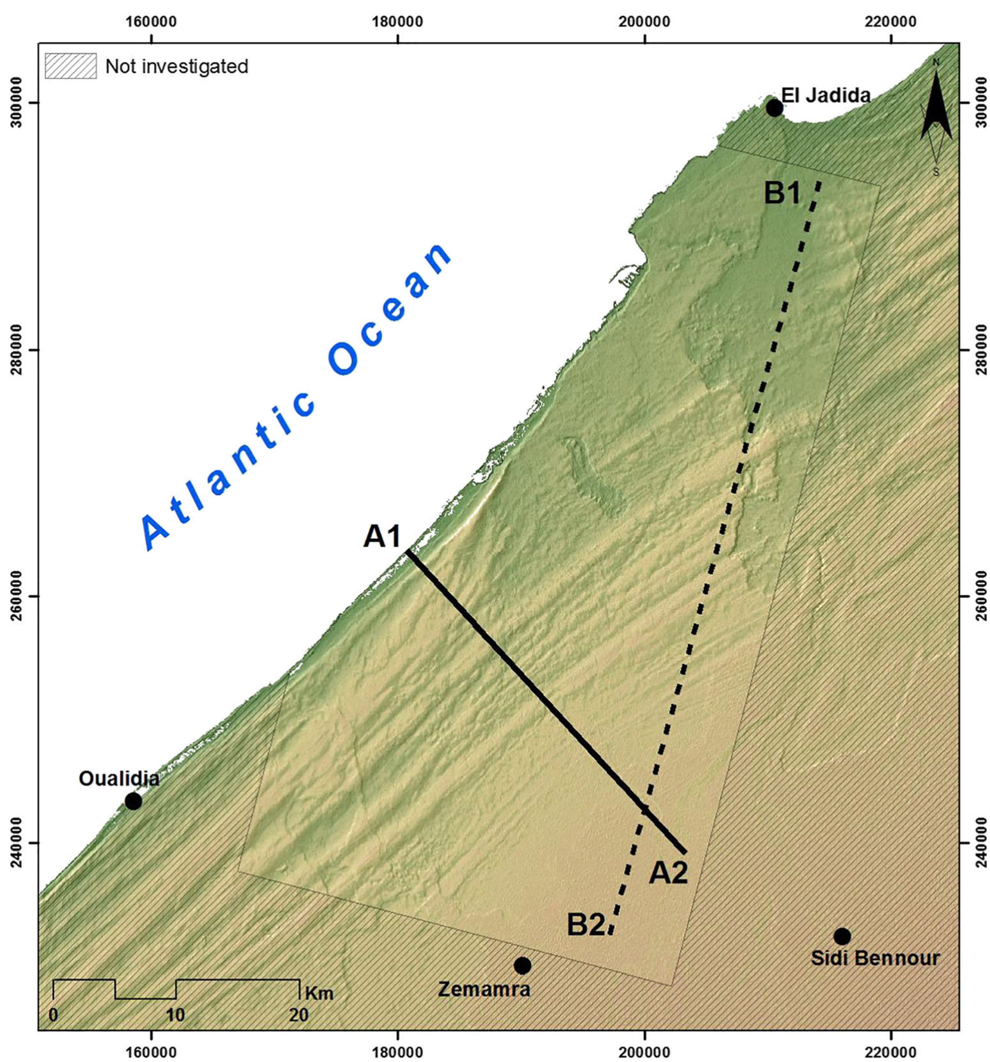

Fig. 9 The situation of elevation profiles A_1A_2 (solid line) and B_1B_2 (dashed line)

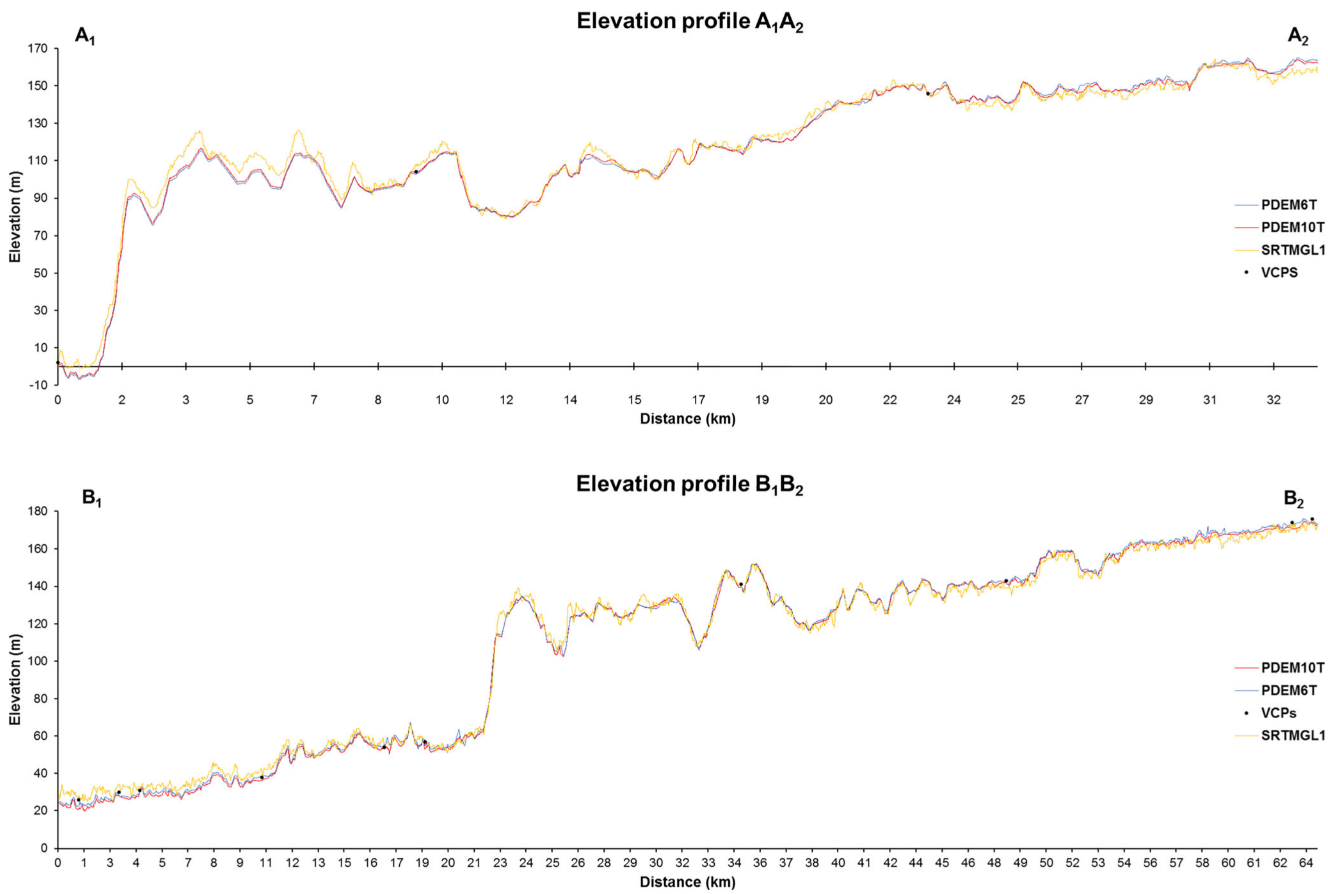

Fig. 10 Elevation profiles comparison between PDEM6T, PDEM10T, SRTMGL1 and VCPs

Until now, the used accuracy assessment techniques are giving an idea just about the vertical accuracy without any information about the planimetric accuracy of the generated PDEMs. To overcome this issue, a qualitative assessment of the planimetric accuracy was performed by comparing the elevation profiles of PDEM6T, PDEM10T, SRTMGL1, and VCPs. Two profiles were chosen based on the area covering all geomorphological units such as Wetlands (Oulja), cliffs, dunes of the Sahel, and the plain of Doukkala, with both low and high gradients. These profiles called Profile A_1A_2 and Profile B_1B_2 are oriented in NW-SE and NNE-SSW respectively (Fig. 9).

PDEM6T, PDEM10T, and SRTMGL1 are illustrated as elevation curves in blue, red, and orange respectively, according to profile's directions, while VCPs are superposed on them with black dots (Fig. 10).

In Profile A_1A_2, the three curves can be divided into two parts. In the first part which represents a hilly region (with the presence of wetlands, such as Sidi Moussa Lagoon, and Dunes of the Sahel), SRTMGL1 is higher than PDEM6T and PDEM10T,

Fig. 11 Example of noise affecting PDEM6T curve and staircase pattern presenting in SRTMGL1 curve

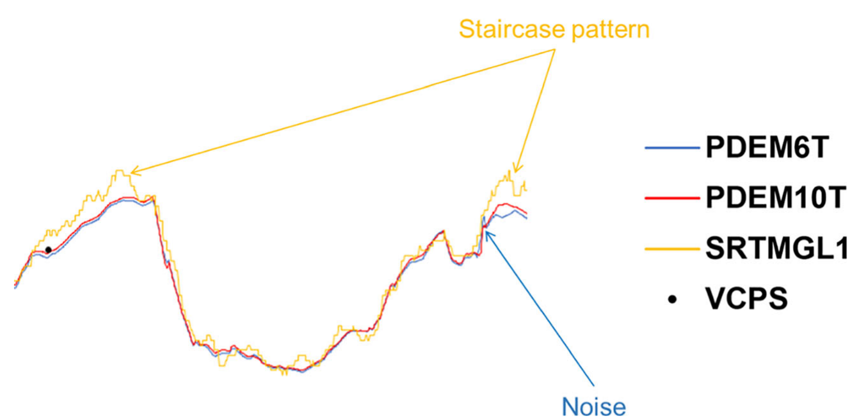

Table 8 Statistical parameters between VCPs, PDEM6T, PDEM10T, and SRTM

	Min (m) Meters	Max (m)	Mean (m)	Median (m)	SD (m)	MAE (m)	$RMSE_Z$ (m)	ACC_z 95 (m)
VCPs – SRTMGL1	-8.000	5.000	0.081	0.000	2.360	1.825	2.286	4.481
VCPs - PDEM6T	-3.246	8.896	0.629	0.671	1.736	1.281	1.841	3.608
VCPs - PDEM10T	-4.021	8.525	0.912	0.750	1.762	1.462	1.978	3.877

but it is observed that SRTMGL1 takes the same shape as PDEM6T and PDEM10T in steep slopes. While in the second part, it is observed that SRTMGL1 fluctuate along PDEM6T and PDEM10T, and in some sections, located in the plain of Doukkala (flat area), SRTMGL1 becomes lower than PDEM6T and PDEM10T. In profile B_1B_2, the difference is less marked and SRTMGL1 is neighboring to PDEM6T and PDEM10T, but the overall shape presents the same aspect as the profile A_1A_2.

Due to its low spatial resolution, SRTMGL1 fails in representing local topographic variations, and therefore, a general shape of the topographic surface is considered. Moreover, the SRTMGL1 landform curves are shown in a staircase pattern with a lot of noise, unlike PDEM6T and PDEM10T curves which show a smoother shape with less noise (Fig. 11).

In the absence of an accurate reference DEM, it is difficult to decide between the exactness of SRTMGL1 and PDEM6T/PDEM10T. To solve this problem, VCPs (as they are the most accurate data we were able to get) were introduced and intersecting with the transect line into DEMs curves in profiles A_1A_2 and B_1B_2. Observing the DEMs curves and the location of VCPs, these show the best fit with PDEM6T and PDEM10T, which indicates that PDEM6T and PDEM10T are more accurate and closest to bare earth than SRTMGL1.

In order to check the accuracy between SRTMGL1 and PDEM6T/PDEM10T and try to find which of them is more accurate according to VCPs, a statistical analysis of errors between VCPs, SRTMGL1, PDEM6T, and PDEM10T (Table 8) was performed, where VCPs were considered as reference elevation data. From these statistics, it was observed that SRTMGL1 has a lower vertical accuracy compared to PDEM6T and PDEM10T, which means that PDEM6T and PDEM10T are more accurate than SRTMGL1.

The assessment methods used above gives us information about the vertical accuracy and distribution of errors through a statistical analysis over the whole PDEM without taking any consideration of topographic influence on error propagation. Considering that errors are probably associated with topographic features, some topographic parameters were analyzed in order to evaluate the effect of topographic features on DEM errors distribution.

Slope and aspect; among other topographic features are two of the most important features that can influence and affect the morphological and hydrological pattern of DEM. For this purpose, they represent the recommended variables to analyze the distribution and concentration of certain spatial objects (Blaschke and Strobl 2003; Pulighe and Fava 2013).

Slope and aspect maps for PDEM6T and PDEM10T were generated, and then slope and aspect values at VCPs were extracted from each PDEM. Later, a statistical analysis of PDEM6T and PDEM10T errors were performed for slope classes and aspect directions (Tables 9 and 10 respectively).

The cumulative percentage distribution of slopes shows that more than 95% of the study area has a slope less than 4 degrees. On the basis of this, a value of 4 degrees was chosen as threshold for classifying slope terrain. From Figure 12, it is seen that terrain slope has a significant impact on the vertical accuracy of both PDEMs. In general, elevation error increases with the increase of terrain slope. In the case of PDEM6T, it is observed that the increase of elevation error is approximately twice for terrain with slope greater than 4 degrees compared to terrain with slope less than 4 degrees. On the other hand, PDEM10T present a minimal variation on the vertical accuracy than PDEM6T, with a remarkable enhancement for terrain slopes exceeding 4 degrees. Based on these results, it can be supposed that there is a correlation between the elevation error and terrain slope, which have a significant impact on the vertical accuracy of PDEM6T and PDEM10T.

Table 9 Summary statistics of errors between VCPs and PDEM6T/PDEM10T for different slope classes

	Slope(°)	Min(m)	Max(m)	Mean(m)	Median(m)	SD(m)	MAE(m)	$RMSE_Z$ $(m)_z$	ACC_z 95(m)
VCPs – PDEM6T	*<4*	-3.246	8.896	0.610	0.672	1.679	1.251	1.781	3.490
	>4	-1.863	6.457	1.155	0.666	3.173	2.109	3.064	6.006
VCPs – PDEM10T	*<4*	-4.021	8.525	0.869	0.697	1.762	1.442	1.959	3.840
	>4	0.376	4.791	1.905	1.663	1.547	1.905	2.372	4.649

Table 10 Summary statistics of residuals between VCPs and PDEM6T/PDEM10T for different aspects directions

	Aspect	Nbr. VCPs	Min (m)	Max (m)	Mean (m)	Median (m)	SD (m)	MAE (m)	$RMSE_Z$ $(m)_z$	ACC_z 95 (m)
PDEM6T	*N*	15	-1.419	2.182	0.560	0.373	0.961	0.813	1.082	2.121
	NE	17	-4.021	3.084	0.404	0.713	1.931	1.641	1.916	3.755
	E	19	-2.378	6.049	0.757	0.629	1.655	1.274	1.788	3.504
	SE	26	-2.585	8.525	1.468	1.316	2.159	1.867	2.568	5.033
	S	11	-2.560	2.866	0.663	0.804	1.346	0.696	0.941	1.844
	SW	7	-2.560	2.866	0.663	0.804	1.346	1.220	1.463	2.867
	W	18	-1.073	2.752	1.050	1.263	1.155	1.289	0.902	1.768
	NW	30	-2.264	6.776	1.478	0.688	2.178	0.381	0.573	1.123
PDEM10T	*N*	15	-0.187	4.663	1.117	0.924	1.237	1.163	1.636	3.207
	NE	17	-4.021	6.049	1.177	0.892	2.402	1.935	2.610	5.116
	E	19	-2.378	2.670	0.220	0.137	1.523	1.306	1.498	2.936
	SE	26	-2.585	8.525	1.230	1.223	2.040	1.689	2.348	4.602
	S	11	-2.560	3.107	0.210	0.216	1.730	1.410	1.663	3.259
	SW	7	-1.499	1.705	0.508	0.801	1.071	0.987	1.114	2.183
	W	18	-1.073	3.710	1.175	1.100	1.258	1.427	1.696	3.324
	NW	30	-2.264	6.776	1.018	0.491	1.816	1.395	2.055	4.028

Similarly, the analysis of elevation errors according to terrain aspect leads to similar results, where terrain aspect has a relative impact on the amount of elevation error (Fig. 13). It was found that PDEM6T and PDEM10T slightly differ in term of the amount, and PDEM10T has relatively a higher amount of elevation error, but; unlike PDEM6T, it keeps the same shape for all accuracy estimators such as SD, MAE, $RMSE_Z$ and ACC_z95. Contrasting to PDEM10T, where the highest amount of elevation error was perceived on slopes facing NE, SE, S, W and NW, PDEM6T shows an irregular shape of elevation error over the four accuracy estimators (SD, MAE, $RMSE_Z$, ACC_z95), with the biggest error was located on slopes facing NE, SE, SW, W and NW. From above, it can be concluded that terrain aspect has an influence on the vertical accuracy of PRISM DEMs. Furthermore, even if PDEM10T has a slightly high amount of elevation error compared to PDEM6T, it shows a stable shape which indicates its good consistency.

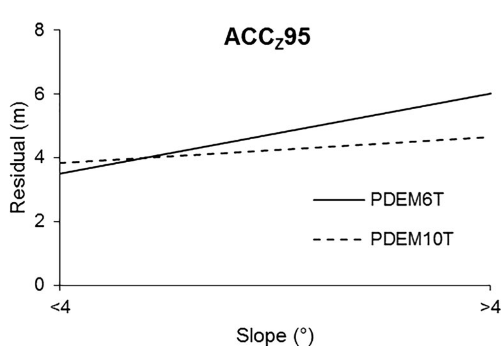

Fig. 12 Influence of slope on the accuracy of PDEM6T and PDEM10T

It can be observed from accuracy results investigated above, that both PDEM6T and PDEM10T have a relatively good accuracy and share similar characteristics. Descriptive statistics and differential errors statistics with VCPs show that PDEM6T is closest to VCPs and has a smallest $RMSE_z$ and ACC_z95 compared to PDEM10T. These results were

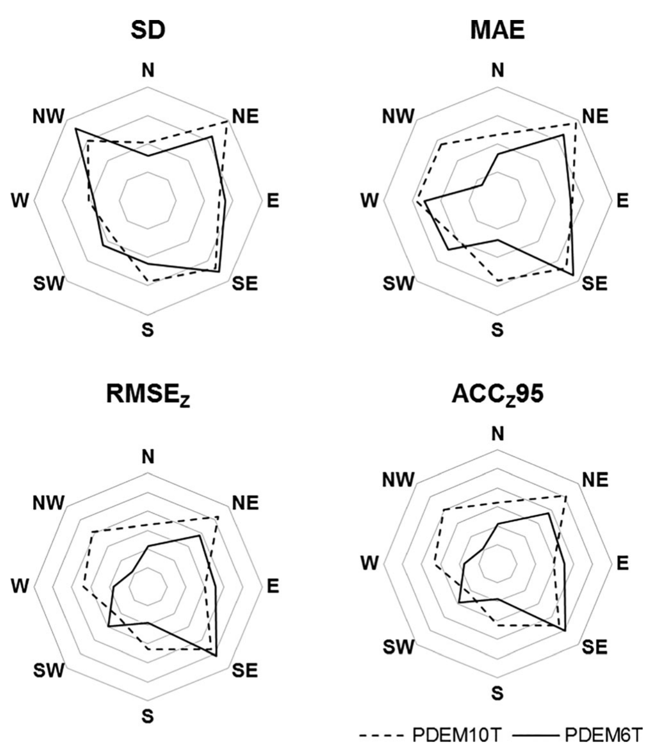

Fig. 13 Relationship between aspect and elevation errors

Table 11 Summary statistics of horizontal errors of PRISM orthoimages

	Min (m)	Max (m)	Mean (m)	Median (m)	SD (m)
Diff. in X (ΔX)	-8.40	8.47	-0.07	-0.30	4.34
Diff. in Y (ΔY)	-10.49	13.69	0.13	-0.77	5.28
Magnitude of Hz diff.	0.94	15.80	5.87	5.54	3.34

confirmed by spatial correlation and regression analysis, which present the highest correlation and determination coefficients in the case of PDEM6T. In contrast to this, image differencing, profiling, and topographic analysis show that PDEM10T presents a better error distribution and it is more consistent and more stable than PDEM6T, which indicates the success of the image matching signifying that artifacts such spikes and outliers in the PDEM10T were minimal.

Based on this, and given the good vertical accuracy which is less than 4 m at 95% confidence level, and also the good consistency of PDEM10T, it was decided to choose it as base DEM for further process.

According to the accuracy guidelines given by the new ASPRS 2014 standard (ASPRS 2015), the reached PDEM10T meets ASPRS Positional Accuracy Standards for Digital Geospatial Data (2014) for a 3.33 m $RMSE_z$ Vertical Accuracy Class, which represents the approximate accuracy of elevation datasets produced from satellite-based sensors.

Concerning the horizontal accuracy of PDEM10T, it equates to the horizontal accuracy class that would apply to planimetric data or digital orthoimagery produced from the same source imagery, using the same orientation solution (ASPRS 2015). In other words, it will be equal to the horizontal accuracy of PRISM orthoimages generated using PDEM10T, which will be defined after the accuracy assessment of PRISM orthoimages.

Later, orthoimages were made for both stereopairs. Using these orthoimages, validation points on them were compared to validation points located on topographic maps. For each location, the difference in X (Easting component) and Y (Northing component) were calculated. Based on these differences, descriptive statistics were calculated such as Min, Max, Mean, and SD (Table 11). From these computations, NSSDA statistics were made, including $RMSE_{xy}$ and NSSDA horizontal accuracy at 95% confidence level (Table 12). Since the horizontal errors are quite similar and independent in each of the x- and y- component (Fig. 14), with an $RMSE_x$ # $RMSE_y$, the horizontal accuracy was calculated using the second case using formula (Eq. 10). Table 12 shows the horizontal errors (shifts) in these locations, while Fig. 15 shows the major directions of these errors and the variability distribution and magnitude of the horizontal errors of validation points.

Table 12 Accuracy statistics of PRISM orthoimages

	Value (m)
$RMSE_x$	4.27
$RMSE_y$	3.65
$RMSE_{xy}$	6.73
$Accuracy_{xy}$ (NSSDA95)	11.60

From these statistics, it can be seen that orthoimages generated using PDEM10T have horizontal $RMSE_{xy}$ of approximately 6.73 m (about 3 pixels) which is equivalent to a horizontal accuracy of 11.60 m (about 5 pixels) at 95% confidence level. Out of 33 validation points, only two points exceed this value. Figure 15 shows the variability distribution and magnitude of the horizontal errors of validation points.

Given these results, and following the NSSDA standards, the obtained accuracy (11.60 m) has to be considered as good, bad, acceptable, or unacceptable, which is a subjective judgment and depends on end users intended applications. Considering the quality of validation points, we think that an accuracy of 11.60 m (5 pixels) is reasonable. According to new ASPRS 2014 standards, the accuracy of these PRISM orthoimages is classified in 5 m $RMSE_x$/$RMSE_y$ Horizontal Accuracy Class, which means that the results of the horizontal accuracy can be defined in map scale of 1:20,000. In cartographic terms, the generated PRISM orthoimages can be used in mapping at 1:25,000 scale.

In summary, a DEM with an $RMSE_z$ of less than 2 m and 4 m vertical accuracy at 95% confidence level was obtained. The horizontal accuracy was achieved from the accuracy assessment of orthoimages which is about 11.6 m at 95% confidence level, with an $RMSE_{xy}$ of about 6.7 m. Those results are consistent with existing studies available in the scientific literature about PRISM derived DEM and orthoimages (Tadono et al. 2007; Bignone and Umakawa 2008; Imai et al. 2008; Maruya and Ohyama 2008; Takaku et al. 2008; Müller et al. 2009; Trisakti et al. 2009).

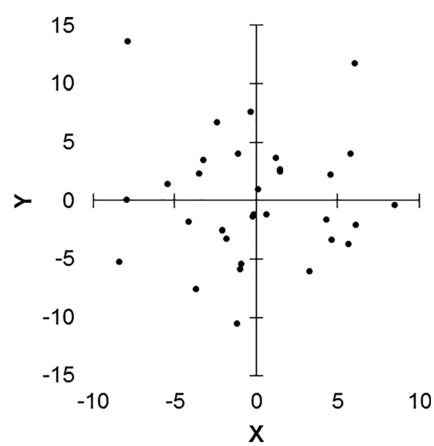

Fig. 14 Spatial distribution of errors of PRIM orhtoimages in X and Y direction

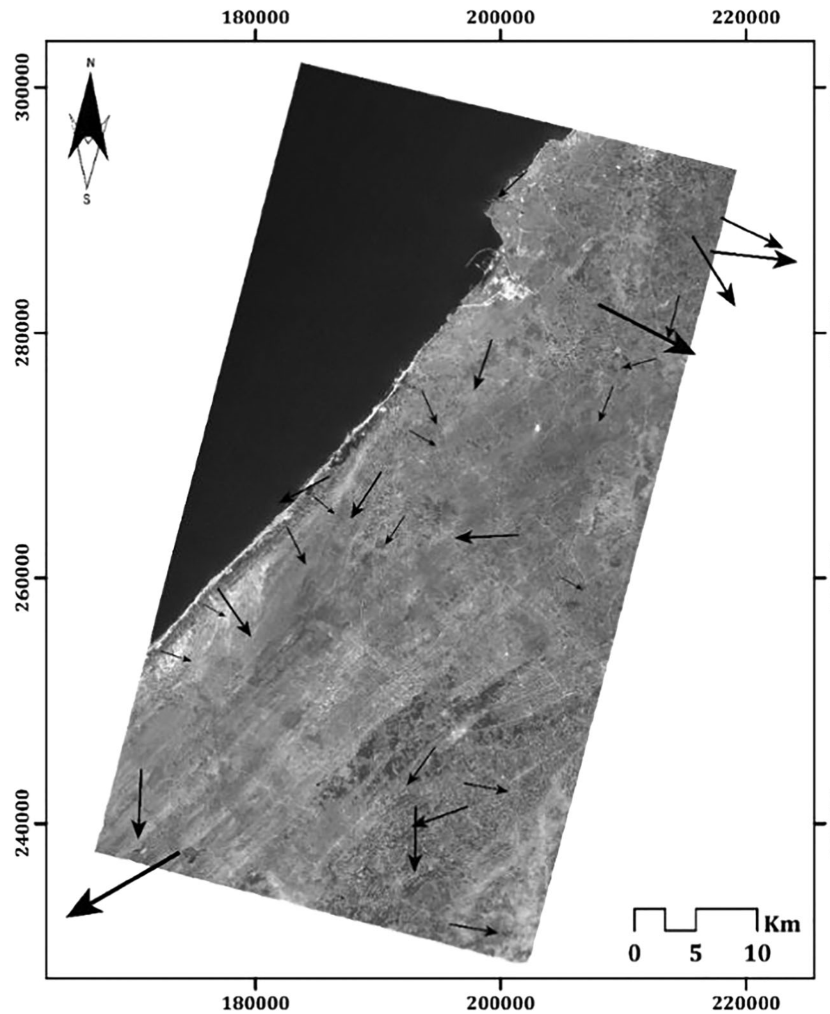

Fig. 15 PRISM orthoimages and directions of the relative magnitude of horizontal error vector (black arrows) of validation points (points were enlarged by a factor of 5)

Conclusion

The idea behind this study was to explore the ability of ALOS-PRISM images in high-resolution DEM generation over the Sahel-Doukkala, as an alternative of available global DEMs such as SRTMGL1 and ASTER GDEM V2, or DEMs generated from digitizing existing topographic maps. Also, the question of the number of required GCPs to improve the accuracy of the model and the generated DEMs was also discussed. In addition, PRISM orthoimages from PRISM DEMs were generated and assessed.

During this work, DEMs covering Sahel-Doukkala were extracted from two sets of ALOS-PRISM images, at 5 m resolution, using zero, 3, 6, 10, and 15 GCPs, obtained from topographic maps at scale 1:25,000. The accuracy assessment was carried out by comparison with 143 well-defined vertical checkpoints and SRTMGL1 using different accuracy assessment techniques. Then, PRISM orthoimages were generated using the extracted PRISM-DEM, and its accuracy was performed in comparison with 33 validation points. The accuracy of generated DEMs and orthoimages was given according to FGDC NSSDA standards.

The obtained results show that a minimum of three GCPs is required in order to adjust the model and to achieve a good vertical and horizontal accuracy of PRISM DEMs over Sahel Doukkala. In contrast to this, increasing the number to ten can stabilize the model which gives a more consistent DEM. Adding more GCPs can improve the model, but with no big difference as it starts to be saturated.

Using ten GCPs, DEM with 3.88 m vertical accuracy at 95% confidence level was obtained. The horizontal accuracy was achieved from the accuracy assessment of orthoimages which is 11.60 m at 95% confidence level. Following the accuracy guidelines of the new ASPRS 2014 standards, these results show that the horizontal accuracy of PRISM-DEM and PRISM orthoimages can be used for mapping at a scale of 1:20,000. The accuracy of obtained DEM and orthoimages remains the best in our study area and is satisfactory for terrain visualization, digital terrain modeling, mapping purposes, spatial analysis, and so on. However, one must be careful because the obtained PDEM still incorporating some points that do not belong to the bare earth. Therefore, the PDEM should be filtered in order to remove all off-terrain points such as trees and buildings, to finally create an accurate DTM, before any terrain modeling and analysis which required bare earth (terrain surface).

In the future, post-processing will be applied on PRISM-DEM so as to derive a DTM for the investigated area. This DTM will be used for further terrain classification and modeling. Also, it will be used for tectono-geomorphological analysis in order to extract lineaments in different distinct landscape and topography, and trying to complete a previous study regarding lineaments extraction and analysis over the study area using multispectral images (Habib et al. 2013).

Results will be extended by using images ALOS-PRISM L1B1 Triplet Mode and try to exploit the respective strengths of each mode, in an attempt to enhance the quality of PRISM-DEM. Furthermore, considering that the uncertainty of reference points is quite high, a DGPS derived points are preferable and would be very useful to improve the overall quality of the DEM generation. Also, independent validation points from DGPS survey will increase the accuracy assessment of the DEM and orthoimages. For this purpose, DGPS surveys fieldwork over Sahel-Doukkala will be planned - if technically possible - in the near future to collect accurate reference points.

Acknowledgements The research reported herein was supported by fellowship given by the National Scientific and Technical Research Center of Morocco (CNRST). ALOS-PRISM images were provided by the European Space Agency (ESA) in the framework of the TIGER initiative.

References

Al-Rousan N, Cheng P, Petrie G et al (1997) Automated DEM Extraction and Orthoimage Generation from SPOT Level 1B Imagery. Photogramm Eng Remote Sens 63:965–974

ASPRS (2015) ASPRS positional accuracy standards for digital geospatial data - edition1 - version 1.0. Photogramm Eng Remote Sens 81:A1–A26. doi:10.14358/PERS.81.3.A1-A26

Bandara K, Samarakoon L, Shrestha RP, Kamiya Y (2011) Automated Generation of Digital Terrain Model Using Point Clouds of Digital Surface Model in Forest Area. Remote Sens 3:845–858. doi: 10.3390/rs3050845

Bhardwaj A (2013) Evaluation of DEM, and orthoimage generated from Cartosat-1 with its potential for feature extraction and visualisation. Am J Remote Sens 1:1–6. doi:10.11648/j.ajrs.20130101.11

Bignone F, Umakawa H (2008) Assessment of ALOS PRISM digital elevation model extraction over Japan. In: ISPRS Archives. XXIst ISPRS Congress Technical Commission V. Vol. XXXVII-B1. Beijing, China, pp 1135–1138

Bitelli G, Girelli VA (2009) Metrical use of declassified satellite imagery for an area of archaeological interest in Turkey. J Cult Herit 10:35–40. doi:10.1016/j.culher.2009.08.004

Blaschke T, Strobl J (2003) Defining landscape units through integrated morphometric characteristics. In: Buhmann E, Ervin S (eds) Landscape modelling: digital techniques for landscape architecture. Wichmann-Verlag, Heidelberg, pp 104–113

Büyüksalih G, Koçak G, Topan H et al (2005) SPOT revisited: accuracy assessment, DEM generation and validation from stereo SPOT 5 HRG images. Photogramm Rec 20:130–146. doi: 10.1111/j.1477-9730.2005.00314.x

Eckert S, Kellenberger T, Itten K (2005) Accuracy assessment of automatically derived digital elevation models from aster data in mountainous terrain. Int J Remote Sens 26:1943–1957. doi:10.1080/0143116042000298306

Fadili A, Mehdi K, Riss J et al (2015) Evaluation of groundwater mineralization processes and seawater intrusion extension in the coastal aquifer of Oualidia, Morocco: hydrochemical and geophysical approach. Arab J Geosci. doi:10.1007/s12517-015-1808-5

Farr TG, Rosen PA, Caro E et al (2007) The shuttle radar topography mission. Rev Geophys 45:1–43. doi:10.1029/2005RG000183

El Bchari F, Theilen-Willige B, Ait Malek H (2014) Remote Sensing and GIS Contribution to the Detection of Coastal Slope Failure in the Safi Area, Morocco. Earth Sci 3:76–84. doi:10.11648/j.earth.20140303.12

Federal Geographic Data Committee (1998) Geospatial positioning accuracy standards, part 3 : National Standard for Spatial Data Accuracy. Virginia

Florinsky IV (2012) Digital terrain analysis in soil science and geology, 1st Editio. Academic Press, Bonston

Galiatsatos N, Donoghue DNM, Philip G (2008) High resolution elevation data derived from stereoscopic CORONA imagery with minimal ground control : an approach using Ikonos and SRTM data. Photogramm Eng Remote Sens 74:1093–1106

Gonçalves J (2005) Assessment of SRTM-3 DEM in Portugal with topographic map data. In: Proceedings of the EARSeL Workshop 3D–Remote Sensing. Porto, Portugal

Gonçalves J (2008) Orientation and DEM extraction from ALOS-PRISM images using the SRTM-DEM as ground control. In: ISPRS Archives. XXIst ISPRS Congress Technical Commission I. Vol. XXXVII-B1. Beijing, China, pp 1177–1181

Habib A, Labbassi K, Akdim N, Tajdi A (2013) Contribution des données ALOS et LANDSAT dans la cartographie et l'analyse des linéaments dans le Sahel Central (Maroc occidental). Rev Française Photogrammétrie Télédétection 203:33–41

Hasegawa H, Matsuo K, Koarai M, et al. (2000) DEM accuracy and the base to height (B/H) ratio of stereo images. In: Fritsch D, Molenaar M (eds) ISPRS Archives. XIXth ISPRS Congress Technical Commission IV. Vol. XXXIII-B4. Amsterdam, The Netherlands, pp 356–359

Hirano A, Welch R, Lang H (2003) Mapping from ASTER stereo image data : DEM validation and accuracy assessment. ISPRS J Photogramm Remote Sens 57:356–370. doi:10.1016/S0924-2716(02)00164-8

Imai Y, Akamatsu Y, Mori M, Shirai N (2008) An accuracy assessment of DSMs and orthoimages derived from ALOS/PRISM and their availability in forestry. In: ISPRS Archives. XXIst ISPRS Congress Technical Commission VIII. Vol. XXXVII-B8. Beijing, China, pp 1021–1026

Jacobsen K (2005) Analyses of SRTM elevation models. In: Proceedings of the EARSeL 3D_Remote Sensing Workshop. Porto, Portugal

Jacobsen K (2013) DEM generation from high resolution satellite imagery. PFG Photogramm Fernerkundung, Geoinf 2013:483–493. doi:10.1127/1432-8364/2013/0194

JAXA (2008) ALOS Data Users Handbook - Revision C

Jordan G (2007) Adaptive smoothing of valleys in DEMs using TIN interpolation from ridgeline elevations : an application to morphotectonic aspect analysis. Comput Geosci 33:573–585. doi:10.1016/j.cageo.2006.08.010

Kääb A (2008) Remote sensing of permafrost-related problems and hazards. Permafr Periglac Process 19:107–136. doi:10.1002/ppp

Khoshelham K (2009) Role of Tie Points in Integrated Sensor Orientation for Photogrammetric Map Compilation. Photogramm Eng Remote Sens 75:305–311

Kocaman S, Gruen A (2009) Orientation and calibration of ALOS/PRISM imagery. In: Heipke C, Jacobsen K, Gerke M (eds) ISPRS archives. XXXVI-1/W51. Hannover, Germany, p 6

Kraus K, Pfeifer N (1998) Determination of terrain models in wooded areas with airborne laser scanner data. ISPRS J Photogramm Remote Sens 53:193–203. doi:10.1016/S0924-2716(98)00009-4

Krauß T, Schneider M, Reinartz P (2009) Orthorectification and DSM generation with ALOS-PRISM data in urban areas. In: Geoscience and Remote Sensing Symposium,2009 I.E. International,IGARSS 2009. IEEE, Cape Town, South Africa, p V-33-V-36

Krauß T, Arefi H, Reinartz P (2011) Evaluation of selected methods for extracting digital terrain models from satellite born digital surface models in urban areas. In: SMPR2011. pp 1–7

Labbassi K, Tajdi A, Er-raji A (2009) Remote sensing and geological mapping for a groundwater recharge model in the arid area of Sebt Brykine: Doukkala, Western Morocco. In: Geoscience and Remote Sensing Symposium,2009 I.E. International,IGARSS 2009. IEEE, Cape Town, South Africa, p I-112-I-115

Lamsal D, Sawagaki T, Watanabe T (2011) Digital terrain modelling using corona and ALOS PRISM data to investigate the distal part of Imja glacier, Khumbu Himal, Nepal. J Mt Sci 8:390–402. doi:10.1007/s11629-011-2064-0

Lane SN, James TD, Crowell MD (2000) Application of digital photogrammetry to complex topography for geomorphological research. Photogramm Rec 16:793–821. doi:10.1111/0031-868X.00152

Leica Geosystems Geospatial Imaging (2006) Leica photogrammetry suite project manager. Leica Geosystems Geospatial Imaging, Norcross

Li Z, Zhi Q, Gold C (2005) Digital terrain modeling: Principales and Methodolgy. CRC Press, Boca Raton, Florida

Maruya M, Ohyama H (2008) Accurate DEM and Ortho-rectified image production from ALOS/PRISM. In: Geoscience and Remote Sensing Symposium, 2008 I.E. International, IGARSS 2008. IEEE, Boston, MA, p I-185-I-188

McCullagh MJ (1988) Terrain and surface modelling systems: theory and practice. Photogramm Rec 12:747–779

Michalis P, Dowman I (2008) Exterior orientation improved by the coplanarity equation and DEM generation for Cartosat-1. In: ISPRS Archives. XXIst ISPRS Congress Technical Commission I. Vol. XXXVII-B1. Xiaohong, Lu, Beijing, China, pp 1301–1307

Migoń P, Kasprzak M (2015) Pathways of geomorphic evolution of sandstone escarpments in the Góry Stołowe tableland (SW Poland) — insights from LiDAR-based high-resolution DEM. Geomorphology. doi:10.1016/j.geomorph.2015.08.022

Milledge DG, Lane SN, Warburton J (2009) Optimization of stereo-matching algorithms using existing DEM data. Photogramm Eng Remote Sens 75:323–333

Mukherjee S, Joshi PK, Mukherjee S et al (2013) Evaluation of vertical accuracy of open source digital elevation model (DEM). Int J Appl Earth Obs Geoinf 21:205–217. doi:10.1016/j.jag.2012.09.004

Müller R, Schneider M, Radhadevi P V, et al. (2009) Stereo evaluation of ALOS PRISM and IKONOS in Yemen. In: Geoscience and Remote Sensing Symposium, 2009 I.E. International, IGARSS 2009. IEEE, Cape Town, South Africa, p II-1-II-2

NASA (2014) U.S. releases enhanced shuttle Land elevation data. http://www2.jpl.nasa.gov/srtm/

NASA JPL (2013) NASA shuttle radar topography mission global 1 arc second - SRTMGL1. NASA LP DAAC, In https://lpdaac.usgs.gov/products/measures_products_table/srtmgl1

Nelson A, Reuter HI, Gessler P (2009) DEM production methods and sources. In: Hengl T, Reuter HI (eds) Geomorphometry: concepts. Software, Applications, Developmen. Elsevier B.V, p 765

Oksanen J (Department of G and CGI (2006) Digital elevation model error in terrain analysis. Faculty of Science - University of Helsinki

Persendt FC, Gomez C (2015) Assessment of drainage network extractions in a low-relief area of the Cuvelai Basin (Namibia) from multiple sources: LiDAR, topographic maps, and digital aerial orthophotographs. Geomorphology. doi:10.1016/j.geomorph.2015.06.047

Pulighe G, Fava F (2013) DEM extraction from archive aerial photos: accuracy assessment in areas of complex topography. Eur J Remote Sens 46:363–378. doi:10.5721/EuJRS20134621

Rabus B, Eineder M, Roth A, Bamler R (2003) The shuttle radar topography mission - a new class of digital elevation models acquired by spaceborne radar. ISPRS J Photogramm Remote Sens 57:241–262. doi:10.1016/S0924-2716(02)00124-7

Rodriguez E, Morris CS, Belz JE, et al (2005) An assessment of the SRTM topographic products, Technical Report JPL D-31639. Pasadena, California

Rozycki S, Wolniewicz W (2007) Accuracy assessment of DSM extracted from IKONOS stereo images. In: Bochenek Z (ed) New developments and challenges in remote sensing. Millpress, Rotterdam, pp 677–683

San BT, Suzen ML (2005) Digital elevation model (DEM) generation and accuracy assessment from ASTER stereo data. Int J Remote Sens 26:5013–5027. doi:10.1080/01431160500177620

Sithole G, Vosselman G (2004) Experimental comparison of filter algorithms for bare-earth extraction from airborne laser scanning point clouds. ISPRS J Photogramm Remote Sens 59:85–101. doi:10.1016/j.isprsjprs.2004.05.004

Tadono T, Shimada M, Watanabe M et al (2004) Calibration and validation of PRISM onboard ALOS. In: Altan O (ed) International archives of photogrammetry. Remote Sensing and Spatial Information Sciences, Istanbul, pp 13–18

Tadono T, Shimada M, Murakami H (2007) Initial calibration results and accuracy assessments of PRISM and AVNIR- onboard ALOS. J Remote Sens Soc Japan 27:329–343

Takaku J, Tadono T, Shimada M (2008) High resolution DSM generation from ALOS PRISM - Calibration Updates -. In: Geoscience and Remote Sensing Symposium, 2008. IGARSS 2008. IEEE International. IEEE, Boston, MA, p I-181-I-184

Theilen-Willige B, Löwner R, El Bchari F, et al (2014) Remote sensing and GIS contribution to the detection of areas susceptible to natural hazards in the Safi area, W-Morocco. In: 2014 1st international conference on information and communication Technologies for Disaster Management (ICT-DM). IEEE, Algiers, Algeria, pp 1–5

Toutin T (2001) Geometric processing of Ikonos geo images with DEM. In: ISPRS Workshop "High Resolution Mapping from Space 2001." Hannover, Germany, pp 1–9

Toutin T (2004) DTM generation from Ikonos in-track stereo images using a 3D physical model. Photogramm Eng Remote Sensing 70: 695–702. doi:10.14358/PERS.70.6.695

Trisakti B, Carolita I, Pradana FA (2009) Digital elevation model from PRISM-ALOS and ASTER stereoscopic data. Int J Remote Sens Earth Sci 6:29–38

Vosselman G (2000) Slope based filtering of laser altimetry data. International Archives of Photogrammetry and Remote Sensing, In, pp 935–942

Wang Y, Yang X, Xu F, et al. (2008) An operational system for sensor modeling and DEM generation of satellite pushbroom sensor images. In: ISPRS Archives. XXIst ISPRS Congress Technical Commission I. Vol. XXXVII-B1. Beijing, China, pp 745–750

Wegmann H (2002) Image orientation by combined (A) AT with GPS and IMU. In: Morain S, Budge A (eds) Proceedings of ISPRS Comission I mid-term symposium: integrated remote sensing at the global. Regional and Local Scale, Denver, CO USA, p 6